https://doi.org/10.5194/egusphere-2024-2280
Preprint. Discussion started: 3 September 2024


# Mount Pinatubo's effect on the moisture-based drivers of plant productivity

Ram Singh[1,2], Kostas Tsigaridis[1,2], Diana Bull[3], Laura P Swiler[3], Benjamin M Wagman[3], Kate Marvel[2]

**Affiliations**

[1] *Center for Climate Systems Research, Columbia University, New York, USA*

[2] *NASA Goddard Institute for Space Studies, New York, NY-10025, USA*

[3] *Sandia National Laboratories, Albuquerque, NM, USA*

**Correspondence:** Ram Singh (rs4068@columbia.edu, ram.bhari85@gmail.com)

## Abstract

Large volcanic eruptions can significantly affect the state of the climate, including stratospheric sulfate concentrations, surface and top-of-atmosphere radiative fluxes, stratospheric and surface temperature, and regional hydroclimate. The prevalence of higher natural variability in how the regional rainfall responds to the volcanic-induced climate perturbations creates a knowledge gap in understanding of how eruptions affect ecohydrological conditions and plant productivity. Here we will explore the understudied store (soil moisture) and flux (evapotranspiration) of water as the short-term ecohydrological control over plant productivity in response to the 1991 eruption of Mt. Pinatubo. We used the NASA's Earth system model for modeling of the 1991's Mt. Pinatubo eruption and detection of hydroclimate response. The model simulates a radiative perturbation of -5 $Wm^{-2}$ and mean surface cooling of ~ 0.5 °C following the Mt. Pinatubo eruption in 1991. The rainfall response is spatially heterogenous, due to dominating variability, yet still shows suppressed rainfall in the northern hemisphere after the eruption. We find that up to 10-15% of land regions show a statistically significant agricultural response. Results confirm that these higher-order impacts successfully present a more robust understanding of inferred plant productivity impacts. Our results also explain the geographical dependence of various contributing factors to the

https://doi.org/10.5194/egusphere-2024-2280
Preprint. Discussion started: 3 September 2024


compound response and their implications for exploring the climate impacts of such episodic forcings.

## Introduction

Volcanic eruptions are the most prominent source of sulfate aerosols in the stratosphere and are among the natural drivers of climate variability. Volcanically-injected sulfate aerosols in the stratosphere alter the Earth's radiative balance by simultaneously reflecting incoming solar radiation and absorbing outgoing longwave radiation emitted from the Earth's surface (Robock, 2000). The presence of sulfate aerosol for months to years after an eruption and its microphysical transformation in the stratosphere affect the climate system through numerous direct and indirect effects (Barnes and Hofmann, 1997; Brad Adams et al., 2003; Briffa et al., 1998; Deshler et al., 2003; Lambert et al., 1993; LeGrande et al., 2016; LeGrande and Anchukaitis, 2015; Li et al., 2013; Pinto et al., 1989; Santer et al., 2014; Sigl et al., 2015; Singh et al., 2023; Tejedor et al., 2021; Toohey et al., 2019; Zambri et al., 2017; Zambri and Robock, 2016; Zhao et al., 1995). The Mt. Pinatubo eruption (June 1991) remains the largest eruption in the satellite era, and it has been explicitly documented and analyzed for its radiative and climate impacts. Numerous studies based on satellite observations and supported through different modeling efforts estimated that Mt. Pinatubo injected 10-20 Tg of $SO_2$ at a range of 18-25 km of plume height (Aquila et al., 2012; Bluth et al., 1992; Dhomse et al., 2014; Gao et al., 2023; McGraw et al., 2024; Mills et al., 2016; Sheng et al., 2015a, b; Stenchikov et al., 1998). The radiative impacts of Mt. Pinatubo's eruption estimate an aerosol optical depth of 0.15 for 550 nm wavelength, with an effective radius in the range of 0.16 to 1 micrometer (μm) and net radiative forcing on the order of 5-6 $Wm^{-2}$ (Lacis et al., 1992; Sato et al., 1993; Stenchikov et al., 1998). Estimates of the induced surface cooling range between 0.3-0.7 °C; lower stratosphere warming estimates are in the range

https://doi.org/10.5194/egusphere-2024-2280
Preprint. Discussion started: 3 September 2024


of 2-3 °C (Bluth et al., 1992; Dutton and Christy, 1992; Hansen et al., 1992; Labitzke and McCormick, 1992; Lacis et al., 1992; McCormick and Veiga, 1992; Minnis et al., 1993; Ramachandran et al., 2000; Stenchikov et al., 1998 Hansen et al., 1993).

In this study, we aim to explore the mechanisms by which the Mt. Pinatubo eruption affected the hydroclimatic conditions and water-based drivers of plant productivity. Agricultural productivity is sensitive to changes in temperature and precipitation (Lobell and Field, 2007; Olesen and Bindi, 2002; Rosenzweig and Parry, 1994). Although much work has been devoted to understanding Mt. Pinatubo's impacts on plant productivity, the literature has been dominated by studies focusing on impacts from changes to the quantity and quality of incoming solar radiation (Farquhar and Roderick, 2003; Gu et al., 2002, 2003; Jones and Cox, 2001; Robock, 2005). Proctor et al. (2018) have estimated a decrease in C4 (maize) and C3 (soy, rice, and wheat) agricultural crop production in response to Mt. Pinatubo driven mainly by changes in incoming radiation. Krakauer and Randerson (2003) evaluated the role of surface cooling in reduced NPP (Net Primary Productivity) using tree ring growth patterns following multiple Mt. Pinatubo-sized eruptions in the last millennium. Reduced NPP was found in northern mid to high latitudes while the signal in the lower latitudes and tropics was either not significant or constrained by the other factors. Other studies have further expanded into societal impact research focusing on volcanically induced poor harvest and agricultural productivity over different regions (Hao et al., 2020; Huhtamaa and Helama, 2017; Manning et al., 2017; Singh et al., 2023; Toohey et al., 2016).

Similarly, much work has been devoted to understanding the hydroclimate response to Mt. Pinatubo through changes in atmospheric precipitation (Barnes et al., 2016; Paik et al., 2020; Trenberth and Dai, 2007). Monsoon seasonal rainfall decreases in the season after an eruption

https://doi.org/10.5194/egusphere-2024-2280
Preprint. Discussion started: 3 September 2024


(Colose et al., 2016; Iles et al., 2013; Liu et al., 2016; Singh et al., 2023; Tejedor et al., 2021). However, rainfall alone provides an incomplete understanding of the drought conditions relevant for plant productivity; a rainfall deficit could in principle be overcome by moisture stored in soil. Hence, meteorological drought indices (e.g. SPI (McKee et al., 1993) or PDSI (Palmer 1965)) based on rainfall ignore a full water balance approach. Furthermore, meteorological drought indices tend to be designed to evaluate prolonged periods of abnormally dry weather conditions. For instance, PDSI is an indicator of drought with a 9-month horizon (Mullapudi et al., 2023). Yet, agricultural crops are heterogeneously sensitive to the timing and degree of moisture deficits during particular portions of the crop growth cycle; for instance, corn yield can be decreased by as much as 25% for a 10% water deficit during the pollination stage (Hane and Pumphrey, 1984). Thus, consideration of indices with high temporal frequency can be especially important when focusing on agriculture.

Soil moisture is the stock of water stored underground and is a primary source for the flux of water to the atmosphere and plants through evapotranspiration. Energetically, evaporation of water from bare surface soil or transpiration of water during photosynthesis in plants from the root zone soils is demanding, using a dominant portion of absorbed solar energy (Trenberth et al., 2009). Plant transpiration is the largest contributor to land evapotranspiration (Nilson and Assmann, 2007; Seneviratne et al., 2010 and references therein). Soil moisture decrease in the root zone establishes an important control over plant productivity as transpiration is an integral component of photosynthesis (Chen and Coughenour, 2004; Denissen et al., 2022). Multiple studies have established that water supply is the limiting factor for climatic evapotranspiration over tropical and subtropical land areas while temperature is an important controlling factor in northern mid- and high latitudes (Dong and Dai, 2017 and references therein). However, soil

https://doi.org/10.5194/egusphere-2024-2280
Preprint. Discussion started: 3 September 2024


moisture changes in response to Mt. Pinatubo eruption (1991) are largely underreported in the literature and it is unclear how soil moisture would respond given volcanically forced changes in primary drivers (temperature and precipitation).

To our knowledge, no study has yet investigated multiple indicators of water use with agricultural productivity after a short-duration event like Mt. Pinatubo eruption. Hence, this study looks to explicitly investigate changes in agricultural drought indices from Mt. Pinatubo by considering the store (soil moisture) and flux (evapotranspiration) of water as potential short-term controls over productivity in particular regions. We use NASA's state-of-the-art Earth system model with interactive aerosol chemistry to conduct the simulation experiments consistent with the counterfactual inference of causation approach for the Mt. Pinatubo eruption. The Mt. Pinatubo effect in the model-simulated climate is evaluated through the various pathways of climate impacts, from the primary dependent variables to the higher order responses controlling plant productivity. Considering the complexity of modeling the terrestrial system, vegetation demographics, and physiological characteristics, we use the soil moisture and evapotranspiration-based agricultural drought indices SMDI (soil moisture deficit index) and ETDI (evapotranspiration deficit index) developed by (Narasimhan and Srinivasan, 2005) to account for agricultural productivity. We evaluate short-term (weekly) and long-term (seasonal) scale changes in SMDI and ETDI relative to statistics over longer modern time-period. By focusing on soil moisture and evapotranspiration metrics, the major water-based drivers of plant productivity are explored to deepen our understanding of the impacts Mt. Pinatubo had on plant productivity.

## 2.0 Method, Experiment, and Data

https://doi.org/10.5194/egusphere-2024-2280
Preprint. Discussion started: 3 September 2024


**2.1 NASA GISS ModelE2.1 (MATRIX)**: We use the state-of-the-art Earth system model from the NASA (National Aeronautics and Space Administration) Goddard Institute for Space Studies, NASA GISS ModelE2.1 (Bauer et al., 2020; Kelley et al., 2020). NASA GISS ModelE2.1 has an atmospheric horizontal latitude-longitude grid spacing of 2.0x2.5 degrees (at the equator) with 40 vertical levels and a model top of 0.1 hPa. We used the interactive chemistry version MATRIX (Multiconfiguration Aerosol TRacker of mIXing state) aerosol microphysics module (Bauer et al., 2008, 2020), which is based on the Quadrature Method of Moment (QMOM) to predict aerosol particle number, mass, and size distribution for 16 different mixed modes of the aerosol population. New particle formation is represented by Vehkamäki et al. (2002), along with aerosol-phase chemistry, condensational growth, coagulation, and mixing states (Bauer et al., 2013). 16 mixing states with 51 aerosol tracers for sulfate, nitrate, ammonium, aerosol water, black carbon, organic carbon, sea salt, and mineral dust are resolved in this microphysical module (Bauer et al., 2008, 2020). The first indirect effect of aerosols in terms of changes in cloud properties through nucleation is also computed within MATRIX.

The ocean component (GISS Ocean v1) of the model has a horizontal resolution of 1x1.25 degrees, with 40 vertical layers. The land component is the Ent Terrestrial Biosphere Model (TBM) (Kim et al., 2015; Kiang 2012) which includes an interactive carbon cycle (Ito et al., 2020), satellite-derived (MODIS) plant functional type and monthly variation of leaf area index (Gao et al., 2008; Myneni et al., 2002), and tree height (Simard et al., 2011). Interannual variations in the vegetation properties are controlled by rescaling the vegetation fraction (Figure S6) using historical crops and pasture at grid scale to account for land cover and land use changes (Ito et al., 2020; Miller et al., 2020). The land model has two defined tiles for the soil layer: bare and vegetated, and each has six vertical levels to a depth of 3.5 m (11.5 feet)

https://doi.org/10.5194/egusphere-2024-2280
Preprint. Discussion started: 3 September 2024


(Rosenzweig and Abramopoulos, 1997). Rooting depth for different plant functional type are also given by Rosenzweig and Abramopoulos (1997) and more than 60% of roots for crop plant functional type are located within 0.6 m (1.96 feet) of soil depth. In this version of the model, for the agricultural grid cells, crop plant functional type and crop calendar are prescribed according to McDermid et al., (2019). Irrigation in the GISS ModelE is implemented using the water irrigation demand data (IWD; (Wisser et al., 2010) and irrigation potential calculations based on (Wada et al., 2013) as discussed in (Cook et al., 2020).

**2.2 Experiment Design**: The MATRIX version of GISS ModelE2.1 with active tracers is three times more computationally expensive than the non-interactive (prescribed pre-calculated aerosol concentration and extinction) version. We extended an equilibrated 1400-yearlong PI control run with non-interactive tracers with an additional 500 years using the MATRIX version with prognostic tracers before starting the 'historical' run. MATRIX includes the tropospheric chemistry scheme that includes the inorganic (Ox NOx Hox and CO), organic chemistry of CH4, and higher hydrocarbons (Gery et al., 1989; Shindell, 2001; Shindell et al., 2003). The stratospheric chemistry includes bromine, chlorine, and polar stratospheric clouds (Shindell et al., 2006). Dust emission in the model is controlled by the climate variables such as winds and soil moisture at the spatial and temporal scales (Miller et al., 2006). However, anthropogenic dust is not included in GISS ModelE2.1. Other anthropogenic emissions, including biomass burning (pre-1997 from (van Marle et al., 2017) and 1997 onwards from the GFED4s inventory (van der Werf et al., 2017)), are taken from the Community Emission Data System (CEDS) inventory (Hoesly et al., 2018). Most importantly, the volcanic $SO_2$ forcing for the 'historical' run (1850-1977) is the daily emission rate from VolcanEESM (Neely and Schmidt 2016 : https://catalogue.ceda.ac.uk/uuid/a8a7e52b299a46c9b09d8e56b283d385 ) and satellite

https://doi.org/10.5194/egusphere-2024-2280
Preprint. Discussion started: 3 September 2024


measurement driven $SO_2$ inventory (Carn et al., 2017) for 1978 to 2022. The cumulative Mt. Pinatubo emission is 15194 kt (~15.2 Tg) of $SO_2$ injected from 12$^{th}$ to 16$^{th}$ of June 1991 above the Mt. Pinatubo vent, with a maximum of 15000 kt (15 Tg) emitted on June 15th at a plume height of 25 km (Diehl et al., 2012). The MATRIX version of the GISS ModelE2.1 used for all of our simulations predicts the nucleation, evolution, and removal of sulfate aerosols prognostically.

Table 1: Simulation experiment design.

| **EXP Name** | **Description** | **Time period /run length** | **Ensembles** | **Configuration** |
|---|---|---|---|---|
| GISS-CMIP6-PI | Preindustrial | 1850 climatology /1300 years | 1 | GISS ModelE2.1 – MATRIX with prescribed stratospheric aerosols (average volcanic AOD for historical period, 1850-2014) |
| GISS-PI | Preindustrial | 1850 climatology /500 years | 1 | Extension to GISS-CMIP6-PI using GISS ModelE2.1 – MATRIX with prognostic tracers |
| GISS-HIST-$SO_2$ | historical | 1850-2014 /165 years | 1 | GISS ModelE2.1 – MATRIX with all forcings as specified by CMIP6 except daily emission rate of injection of $SO_2$ (VolcanEESM; Neely & Schmidt 2016; Carn et al., 2017) |
| GISS-PIN-$SO_2$ | historical | 1986-1999 / 15 years | 11* | GISS ModelE2.1 – MATRIX Branched out from GISS-HIST-SO2, with all forcings as specified by CMIP6 except daily emission rate of $SO_2$ from a combination of VolcanEESM (Neely & Schmidt 2016) and Carn et al., 2017. |
| GISS-NOPIN-$SO_2$ | historical | 1986-1999 / 15 years | 11* | GISS ModelE2.1 – MATRIX with all forcings as according to CMIP6 with daily emission rate |

https://doi.org/10.5194/egusphere-2024-2280
Preprint. Discussion started: 3 September 2024


| | | | | |
|---|---|---|---|---|
| | | | | of $SO_2$ **without Mt. Pinatubo** from a combination of VolcanEESM (Neely & Schmidt 2016) and Carn et al., 2017. |

*These ensemble members are branched out from the GISS-HIST-$SO_2$ by perturbing a radiation-related random number generator that deals with fractional cloudiness in the column.

**2.3 Methods:** This study aims to explore the impacts of the Mt. Pinatubo eruption on the major drivers of primary productivity, focusing on soil moisture-related metrics and evapotranspiration. Hereafter, we use the terminology 'PCH' (Mt. Pinatubo and Cerro Hudson) to refer to the 'GISS-PIN-SO2' and 'NP' for the counter-factual ensemble 'GISS-NOPIN-SO2'. Since we are focusing on the Mt. Pinatubo driven climate response, we have included the Cerro Hudson eruption in both ensembles.

**2.3.1 Statistical analysis used to detect Mt. Pinatubo-significant regions and calculate their anomalies.**

We treat the no-Pinatubo ensemble (NP) as a counter-factual climate simulation and utilize it to perform the paired Student's t-test. The null hypothesis is that the ensemble means of a quantity of interest (QoI) in a region over a time period are the same between ensembles: $H_o: \bar{\mu}_{PCH} = \bar{\mu}_{NP}$. Regions filled in grey in subsequent figures in this document indicate that the null hypothesis cannot be rejected at the 95% confidence level. Regions in which the null hypothesis is not accepted are highlighted in color in subsequent plots, where the color hues show anomalies with respect to the simulated historical climatology for the period 1950-2014. The coloring is done to emphasize significant regions of anomalies, but we emphasize the difference in calculations: the grey regions show no significant change between the PCH and NP ensembles, while the anomalies are PCH ensemble mean minus climatology.

**2.4 Impact metrics**

https://doi.org/10.5194/egusphere-2024-2280
Preprint. Discussion started: 3 September 2024


The distribution of incoming and outgoing radiation influences the hydrological cycle (Kiehl and Trenberth, 1997; Trenberth and Dai, 2007). A reduction of solar radiation at the surface has the potential to reduce rainfall and change the latent heat-dominated atmospheric heating pattern (Trenberth and Stepaniak, 2004). The perturbed atmospheric conditions and surface energy budget could affect soil moisture. Along with the surface air temperature and precipitation, we use soil moisture and surface energy budget-oriented drought indices (the soil moisture deficit index (SMDI) and evapotranspiration deficit index (ETDI)) to evaluate the land-atmosphere interaction and account for the potential drivers to the crop plant productivity in the model simulated post- Mt. Pinatubo environmental conditions (Narasimhan and Srinivasan 2005). SMDI represents the land-based soil moisture state in selected depth horizons (i.e. SMDI_2 means Soil Moisture Deficit Index for 2 feet (0.6 m) depth). ETDI represents the atmospheric conditions governing the land-atmosphere interaction and is an indicator of plant health. Lastly, plant transpiration is analyzed to the explore the simulated physiological response to the volcanically induced hydroclimatic conditions.

The Palmer drought severity index (PDSI) and other indices are commonly used to represent climatological drought conditions, but we focus on SMDI and ETDI because these can represent short-term developing agricultural drought conditions as a response to plant productivity and are free from the limitations of other metrics like PDSI. For example, SMDI and ETDI are seasonally independent measures and are comparable across space, even for different climatic zones.

SMDI and ETDI were calculated as described in Narasimhan and Srinivasan (2005) using model output at monthly and daily scales. Daily model output is resampled weekly to compute the indices. Weekly frequency is used because it is suitable for agricultural applications and the

https://doi.org/10.5194/egusphere-2024-2280
Preprint. Discussion started: 3 September 2024


daily frequency is comparatively higher and computationally expensive for such indices. Below we reproduce the weekly calculation of SMDI and ETDI as presented in Narasimhan and Srinivasan (2005).

**2.4.1 Soil Moisture Deficit Indices (SMDI)** : Soil moisture deficit index measures the wetness/dryness of the soil moisture condition in comparison to long term records spanning 1950-2014.

$$SD_{i,j} = \frac{SW_{i,j} - MSW_j}{MSW_j - minSW_j} \times 100 \quad \text{if } SW_{i,j} \leq MSW_j \qquad \text{..... (2.4.1a)}$$

And

$$SD_{i,j} = \frac{SW_{i,j} - MSW_j}{maxSW_j - MSW_j} \times 100 \quad \text{if } SW_{i,j} > MSW_j \qquad \text{..... (2.4.1b)}$$

$SD_{i,j}$ is the soil water deficit (%) for week j of year i. $SW_{i,j}$ is the mean weekly soil water available in the soil profile (mm) for week j of year i, $MSW_j$ is the long-term (calibration period) median available water in the soil profile (mm) for week j, and $minSW_j$ and $maxSW_j$ are the $j^{th}$ weekly minimum and maximum of soil water available in the soil profile across the calibration period (1950-2014). The soil mositure deficit index for any given week can be calculated as

$$SMDI_j = 0.5 * SMDI_{j-1} + SD_j/50 \qquad \text{..... (2.4.1c)}$$

SMDI can be calculated for different depths of soil; we used the 2, 4 and 6 feet depths for SMDI estimation, approximately 0.6, 1.2, and 1.8 meters, respectively. For SMDI, it is typical to use feet instead of meters in the literature, which is why we use the same units here. SMDI-4 means we considered the soil moisture content between 2 to 4 feet depth. Similarly, SMDI-6 indicates the soil moisture content between 4 to 6 feet in depth.

https://doi.org/10.5194/egusphere-2024-2280
Preprint. Discussion started: 3 September 2024


**2.4.2 Evapotranspiration Deficit Index (ETDI):** The limitations of the Palmer Drought Severity Index (PDSI; Palmer, 1965) and Crop Moisture Index (CMI; (Palmer, 1968)) in the formulation used for PET calculation Thornthwaite, (1948) and lack of accountability to the land cover type on water balance encouraged the exploration of ETDI for agricultural productivity. Also, in the climate models, surface energy fluxes are parameterized in terms of the thermodynamical gradient of atmosphere and land models and thus represent the land-atmosphere interactions not accounted for by these atmosphere-only indices. We utilized model simulated surface energy fluxes (Latent and Sensible heat) to calculate the potential (PET) and actual evapotranspiration (AET) to estimate the water stress ratio. However, the applicability of the Penman-Monteith equation for reference crops Allen et al., (1998) provides a substitute method for PET calculation, which, although not shown, broadly produced similar results. In Equation 2.4.2a and 2.4.2b we used the model simulated energy fluxes to calculate AET and PET as suggested in (Milly and Dunne, 2016; Scheff and Frierson, 2015).

The energy budget equation at the surface is given by Rn= G + LH+SH, where Rn is incoming solar radiation, G is ground energy, LH and SH represent the Latent and Sensible heat fluxes, respectively. We then use these to calculate PET and AET (unit as mm per day):

$$\mathrm{PET} = 0.8(\mathrm{R_n} - \mathrm{G}) = (0.8 * 0.0864/2.45) * (\mathrm{LH} + \mathrm{SH}) \quad \ldots\ldots. \ (2.4.2a)$$

And

$$\mathrm{AET} = \mathrm{LH}^* \ (0.0864/2.45). \quad \ldots\ldots. \ (2.4.2b)$$

The evapotranspiration deficit index is estimated using the water stress condition using the actual evapotranspiration (AET) and potential evapotranspiration (PET) per grid cell as given below.

$$\mathrm{WS} = \frac{\mathrm{PET-AET}}{\mathrm{PET}} \quad \ldots.. \ (2.4.2c)$$

https://doi.org/10.5194/egusphere-2024-2280
Preprint. Discussion started: 3 September 2024


WS ranges between 0 to 1, where 0 signifies that evapotranspiration is happening at potential rate and 1 stands for no actual evapotranspiration. WS represents the water stress ratio at a monthly or weekly basis ($WS_j$), which is further utilized to calculate water stress anomaly ($WSA_{i,j}$) for week j of year i as given below.

$$WSA_{i,j} = \frac{MWS_j - WS_{i,j}}{MWS_j - minWS_j} \times 100 \quad \text{if } WS_{i,j} \leq MWS_j \quad \ldots\ldots (2.4.2d)$$

And

$$WSA_{i,j} = \frac{MWS_j - WS_{i,j}}{maxWS_j - MWS_j} \times 100 \quad \text{if } WS_{i,j} > MWS_j \quad \ldots\ldots. (2.4.2e)$$

Here, $MWS_j$, $minWS_j$, and $maxWS_j$ represent the longterm median, minimum, and maximum of the water stress ratio over the calibration period. Water stress anomaly ranges between -100% to 100%, indicating very dry to wet conditions over the region.

Finally the severity of the drought condition is calculated as ETDI, similar to SMDI (equation 2.4.1c) at a monthly/weekly time scale.

$$ETDI_j = 0.5 * ETDI_{j-1} + WSA_j / 50. \quad \ldots\ldots\ldots (2.4.2f)$$

The indices SMDI and ETDI range from -4 to +4, representing the excessive wet and dry conditions. The bounding values -4 or +4 represent extremely dry/wet conditions as the deficit/excess of soil-moisture deficit (SM) or water stress anomaly (WSA) is reached, relative to the maximum over the reference calibration period.

We also highlight the justification for selecting 1950-2014 as the base period for analyzing the response in climate variables and the long-term calibration period for drought indices calculations. (**Supplementary information** section 1s).

## 3.0 Results

The result section of this study first presents the NASA GISS model's simulated properties of the 1991 Mt. Pinatubo eruption and then further evaluates the primary (aerosol optical depth, radiation, and temperature) and secondary (precipitation, soil moisture, evapotranspiration, and transpiration) impacts on plant productivity.

### 3.1 Radiative forcings and response

We analyze the microphysical and radiative properties of volcanic aerosol simulated by the NASA GISS ModelE (MATRIX) in the PCH ensemble set. The current setup of GISS ModelE uses the aerosol microphysical module MATRIX represent the various states and provide particle number, mass, and size information for different mixed modes of the aerosol population. In the simulation of the Mt. Pinatubo eruption, the volcanically injected $SO_2$ in the stratosphere oxidizes in the presence of prognostically evolving OH radicals to form the stratospheric sulfate aerosols. Sulfate aerosols grow by condensation of gas (nucleation, and self-coagulation (preexisting)) to the Aitken (AKK) mode (mean mass diameter <0.1 µm), and further growth in size leads to the transfer to Accumulation (ACC) mode (Bauer et al., 2008; Bekki, 1995). The transfer between the two particle modes is controlled through the transfer function based on particle mean mass diameter (Bauer et al., 2008). GISS ModelE (MATRIX) PCH simulated a sulfate aerosol size with an effective radius ($R_{eff}$) of the order of 0.3-0.6 µm after the Mt. Pinatubo eruption (not shown), consistent with several observation and modeling estimates (Bauman et al., 2003; Bingen et al., 2004; Russell et al., 1996; Stenchikov et al., 1998). GISS ModelE (MATRIX) PCH simulated a peak global mean aerosol optical depth (AOD; for 550 nm wavelength) of 0.21 (Supplementary Fig S2 bottom panel) a few months after the eruption, which then decreases due to deposition (English et al., 2013; Sato et al., 1993). Here, the model-simulated extinction of the radiation (AOD) due to volcanic aerosol and radiative forcing is larger than previously reported AOD of 0.15 and forcing of -4.0 to -5.0 $Wm^{-2}$ due to the Mt. Pinatubo eruption (Hansen et al., 1992; Lacis et al., 1992).

https://doi.org/10.5194/egusphere-2024-2280
Preprint. Discussion started: 3 September 2024


The mass and size of volcanic sulfate aerosol firmly control the scattering of the incoming shortwave radiation and the absorption of longwave (Brown et al., 2024; Kinne et al., 1992; Lacis, 2015; Lacis et al., 1992; Lacis and Hansen, 1974). The first-order climate response to the volcanically-injected sulfate aerosol in the stratosphere is the perturbation of the radiative balance of the Earth system (Hansen et al., 1980; Lacis et al., 1992; Stenchikov et al., 1998). Figure 1 shows that the GISS ModelE PCH has simulated a peak longwave, shortwave, and net radiative response of +3.0 $Wm^{-2}$, -8.0 $Wm^{-2}$, and -5.0 $Wm^{-2}$ respectively, a few months after the eruption, which recovers slowly in next 24 months and is consistent with previous studies (Stenchikov et al., 1998; Hansen et al., 1992; Minnis et al., 1993; Brown et al 2024). These radiative responses are calculated with respect to the climatology for the period 1950-2014 in GISS-Hist-SO2. The GISS model also simulated a smaller peak ranging within 1 $Wm^{-2}$ in the counterfactual (without Mt. Pinatubo) runs, likely due to the Cerro Hudson eruption in August 1991.

https://doi.org/10.5194/egusphere-2024-2280
Preprint. Discussion started: 3 September 2024


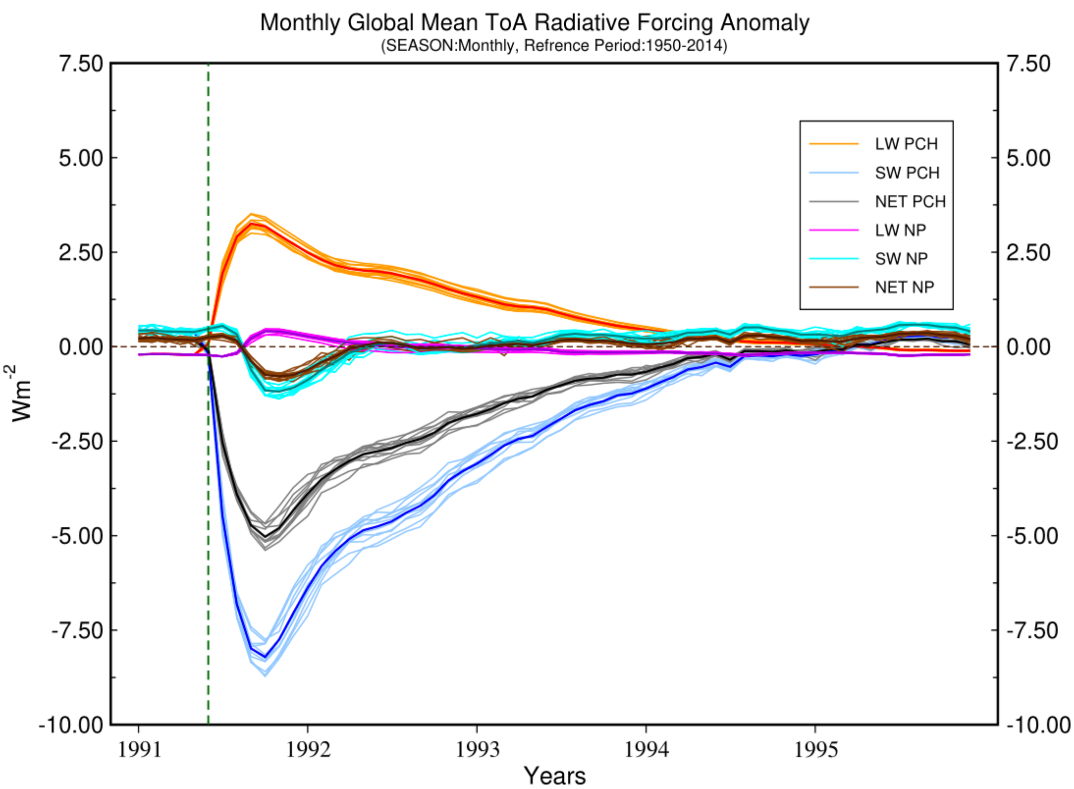


Figure 1. Monthly anomaly of longwave, shortwave, and net radiative forcing simulated by the GISS ModelE for Mt. Pinatubo (PCH) and counterfactual (NP) ensemble. The response anomalies are calculated with respect the climatology for the period 1950-2014, taken from the GISS historical runs (GISS-HIST-SO2). The light-colored thin lines represent the individual ensemble member, and the dark broad line is multi-ensemble mean for each variable (longwave, shortwave and net radiative response).

### 3.2 Aerosol dispersion and Temperature Response

Figure 2 shows the zonal mean anomaly for the aerosol optical depth (AOD), lower stratosphere temperature (MSU-TLS satellite simulator), and surface temperature. The zonal AOD shows the dispersion and transport of aerosol poleward after the eruption. Horizontal dispersion and transport of the aerosols is strictly influenced by the stratospheric meteorology and atmospheric circulation, which is independent in each ensemble member, and depends on the

https://doi.org/10.5194/egusphere-2024-2280
Preprint. Discussion started: 3 September 2024


plume height and season. GISS ModelE has simulated AOD consistently with previous studies (Aquila et al., 2012; Brown et al., 2024; Rogers et al., 1998; Timmreck et al., 1999; Trepte et al., 1993). Cross-equatorial dispersion to the southern hemisphere might be due to the more robust Brewer-Dobson circulation in the austral winter (Aquila et al., 2012). Meanwhile, the phases of QBO and local heating also play a crucial role in the poleward and vertical dispersion of stratospheric aerosols (Hitchman et al., 1994; Ehrmann et al., 2024 (in-prep)). A smaller peak in the southern hemisphere (45° S) in later 1991 likely due to the Cerro Hudson eruption, which injected ~1.5 Tg of $SO_2$ at a height of 15 km.

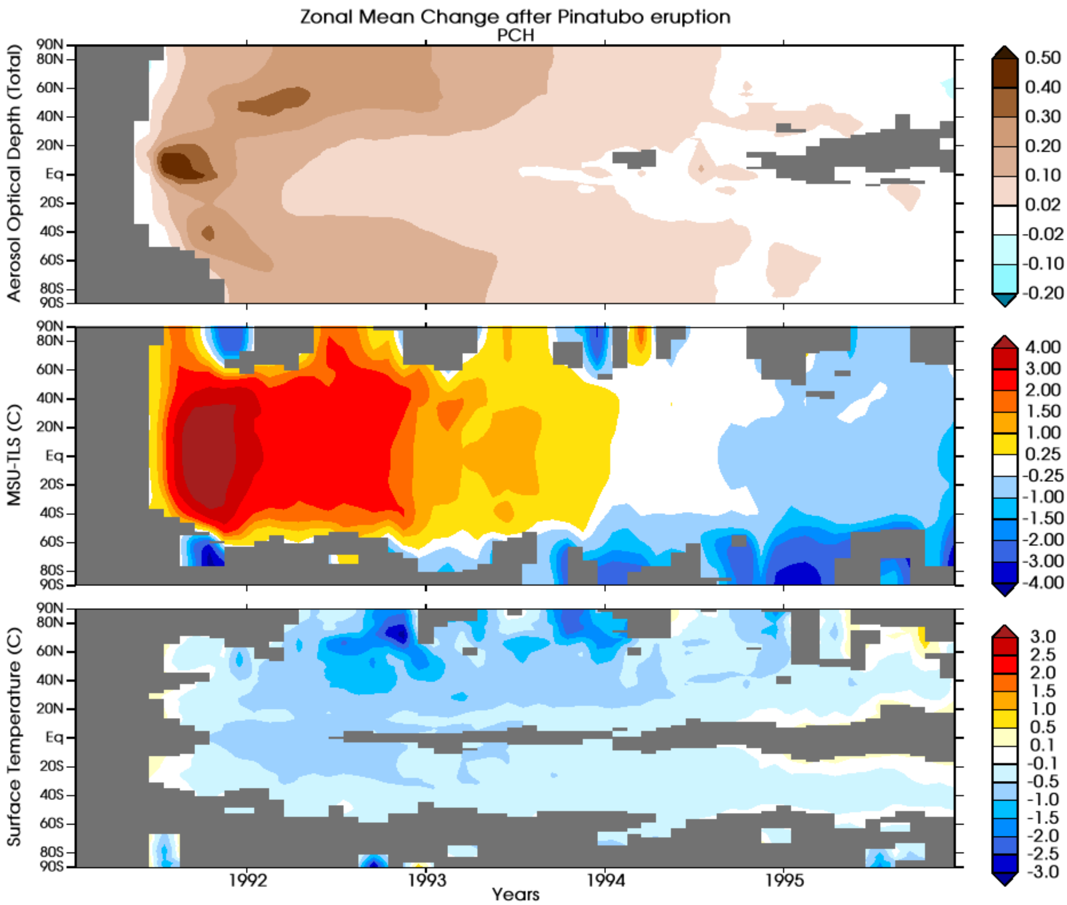

https://doi.org/10.5194/egusphere-2024-2280
Preprint. Discussion started: 3 September 2024


Figure 2. Zonal mean of monthly anomalies for multi ensemble mean for aerosol optical depth at 550 nm (top panel), microwave sounding unit temperature (MSU-TLS) for lower stratosphere (middle panel) and surface air temperature with respect to the 1950-2014 climatology. Gray regions show no statistically significant difference between the PCH and NP response. The colored areas show anomalies of PCH with respect to the climatology from 1950-2014.

The middle and lower panels in Figure 2 show the model-simulated microwave sounding unit (MSU) temperature for the tropical lower stratosphere (TLS) response due to absorption of longwave radiation and for the surface temperature response due to the net radiative perturbation, which is dominated by the scattering of incoming solar radiation. The model simulates a peak warming of over 4 °C in the tropical lower stratosphere shortly after the eruption, which lasts for a few months when the concentration of sulfate aerosols is highest. Significant warming in the range 2-3 °C lasts until the end of 1992, and overall simulated stratospheric warming is consistent with previous studies. Figure S2 (top panel) shows a steplike transition with time with a global mean increase of 3.0 °C in the lower stratosphere temperature after the Mt. Pinatubo eruption followed by a trend consistent with Ramaswamy et al., (2006). The zonal structure of surface temperature shows that the surface cooling follows the aerosol optical depth pattern, and the greatest cooling is simulated in high latitudes. Temporal characteristics of lower stratosphere warming, and surface cooling also show the seasonal variations of sunlight in northern polar latitudes.

The spatial pattern of surface air temperature response is evaluated at the seasonal scale for each year from 1991 to 1995 as shown in Figure 3. We conclude that the volcanic forcing from the Mt. Pinatubo eruption results in a statistically different seasonal mean surface air temperature response. Figure 3 shows that a spatial pattern of surface cooling starts appearing after a few months of the eruption (during the SON season of the year 1991) when the gaseous

https://doi.org/10.5194/egusphere-2024-2280
Preprint. Discussion started: 3 September 2024


$SO_2$ is oxidized into sulfate aerosols. The surface cooling signature due to the volcanic aerosols is significant in 1992 and 1993 before recovering in 1994 towards pre-eruption temperature conditions. The highest surface cooling is noticed over the sub-tropics and higher latitude land regions in the northern hemisphere and reaches up to 2.5 °C at a regional scale.

To summarize: the PCH GISS ModelE simulated global mean peak cooling response is ~0.5 °C after the eruption as shown in Supplement figure S2 (Middle panel) with a range between 0.25 – 1.0 °C for individual ensemble members, and this is consistent with the various observation and modeling studies (Brown et al., 2024; Dutton and Christy, 1992; Hansen et al., 1996; Minnis et al., 1993; Parker et al., 1996; Ramachandran et al., 2000; Stenchikov et al., 1998)( Kirchner et al., 1999).

https://doi.org/10.5194/egusphere-2024-2280
Preprint. Discussion started: 3 September 2024


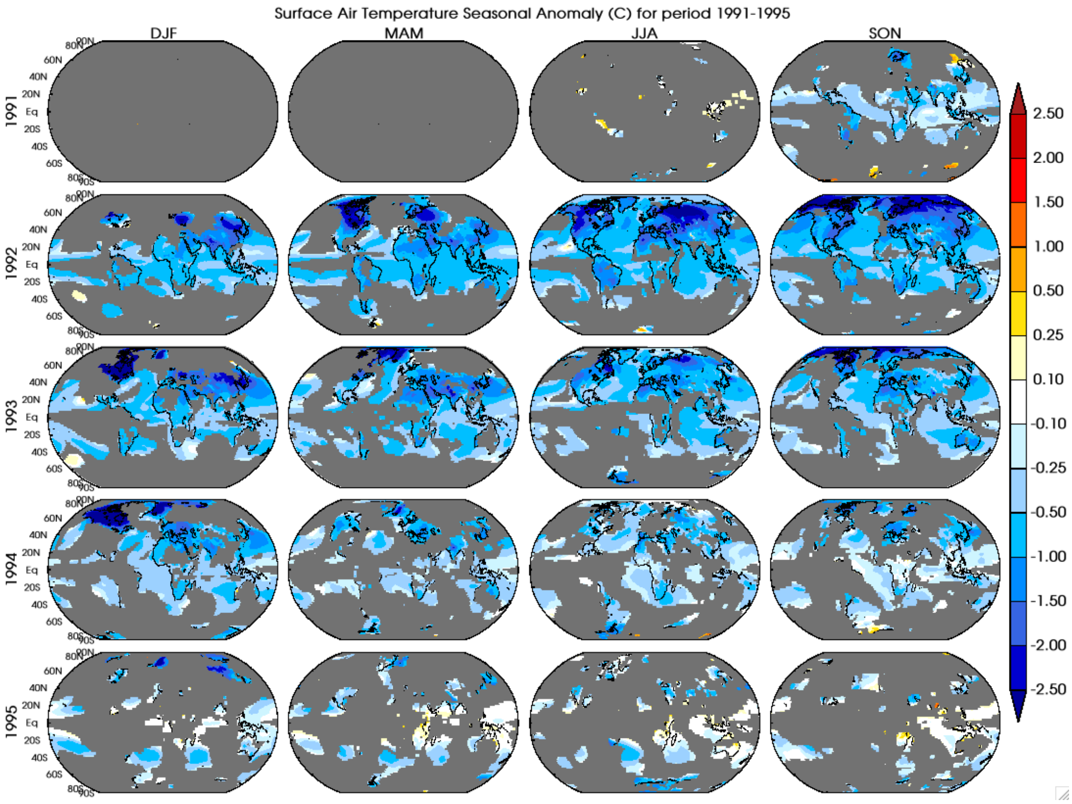


Figure 3: Seasonal mean surface temperature anomalies (°C) from the year 1991 to 1995 with respect to the reference period of 1950-2014. A grey color is painted over the grid cells where the surface temperature anomalies are not statistically significant in comparison to the counter-factual ensemble. The colored areas show anomalies of PCH with respect to the climatology from 1950-2014.

### 3.3 Rainfall Response

Precipitation, presented seasonally for year of eruption (1991) and following year (1992) in Figure 4, shows a highly complex and variable response to the volcanically induced tropospheric cooling and radiative balance perturbation because of its sensitivity to the other climate system components. Studies have shown that global mean precipitation decreases after large volcanic eruptions (Gu et al., 2007; Gu and Adler, 2012; Iles et al., 2013; Robock and Liu,

https://doi.org/10.5194/egusphere-2024-2280
Preprint. Discussion started: 3 September 2024


1994; Singh et al., 2023; Trenberth and Dai, 2007). Colose et al., (2016) have postulated that the asymmetrical surface cooling and radiative balance perturbation create an energetic deficit in the hemisphere of eruption that constrains the poleward propagation of tropical rainfall belt (ITCZ) in that hemisphere. In the case of the Mt. Pinatubo eruption, the PCH simulations show that regional patches of significant decrease of up to 1 mm per day are spotted over tropical and northern hemispheres (Africa, eastern and northern Asia) after the eruption (Figure 4). Also, increasing rainfall patterns are simulated over the Mediterranean and European regions. Broadly, the confidence level of precipitation response due to volcanic aerosols is strongly influenced by the uncertainty due to many possible factors and prominent modes of atmospheric variability, such as the strength of El Nino (Paik et al., 2020).

The zonal mean of the rainfall response (Figure S3) shows a clear decreasing trend in the northern hemisphere tropical and higher latitudes with a positive rainfall response band around 20° N. The PCH modelled rainfall response due to the Mt. Pinatubo eruption is broadly consistent with the previous studies (Joseph and Zeng, 2011; Liu et al., 2016; Trenberth and Dai, 2007), but the uncertainty in rainfall response is still high. Although we use statistical significance as our metric of determining significant anomalies, we do not deny erroneous signals due to the model's internal variability when averaging the impacts across multiple ensembles (Polvani et al., 2019). The inconsistency and complexity in the precipitation response drives us to explore the compound hydroclimatic pathways of impacts beyond the rainfall such as droughts.

https://doi.org/10.5194/egusphere-2024-2280
Preprint. Discussion started: 3 September 2024


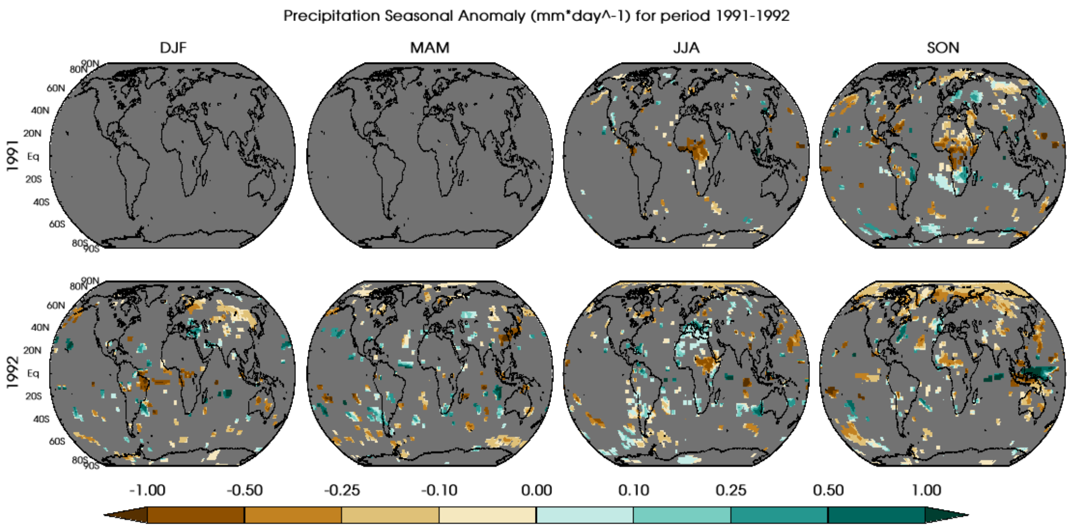


Figure 4. Seasonal mean precipitation anomalies (mm per day) from the year 1991 and 1992 with respect to the reference period of 1950-2014. A grey color is painted over the grid cells where the precipitation anomalies are not statistically significant in comparison to the counter-factual ensemble. The colored areas show anomalies of PCH with respect to the climatology from 1950-2014.

### 3.4 Drought Conditions

Land-atmosphere interaction under a radiatively perturbed environment plays a crucial role in regulating the climate response at regional and sub-regional scales. Changes in land-atmosphere interactions on short timescales can strongly affect plant productivity. Even short-lived adverse conditions in the growth cycle have the potential for outsized impacts, especially if they happen at a particular time in the growing cycle. Hence, we explore the weekly aspects of these drought conditions in Section 4 to explore the temporal characteristics of variability in the conditions.

#### 3.4.1 Seasonal Soil Moisture Drought Index (SMDI)

https://doi.org/10.5194/egusphere-2024-2280
Preprint. Discussion started: 3 September 2024


The root zone is commonly defined as the top 3 – 6 feet of the soil column (Keshavarz et al., 2014, and references therein) but most agricultural crops have shallower root systems confined to the top 2 feet (Narasimhan and Srinivasan 2005). Hence, we focus on the soil moisture deficit index (SMDI) (Narasimhan and Srinivasan 2005) for the top 2 feet of ground depth (SMDI_2) as shown in Figure 5. As anticipated, more land area is covered by statistically different SMDI_2 then in Figure 4 helping to further our analysis of water-driven impact to plant productivity more then with precipitation.

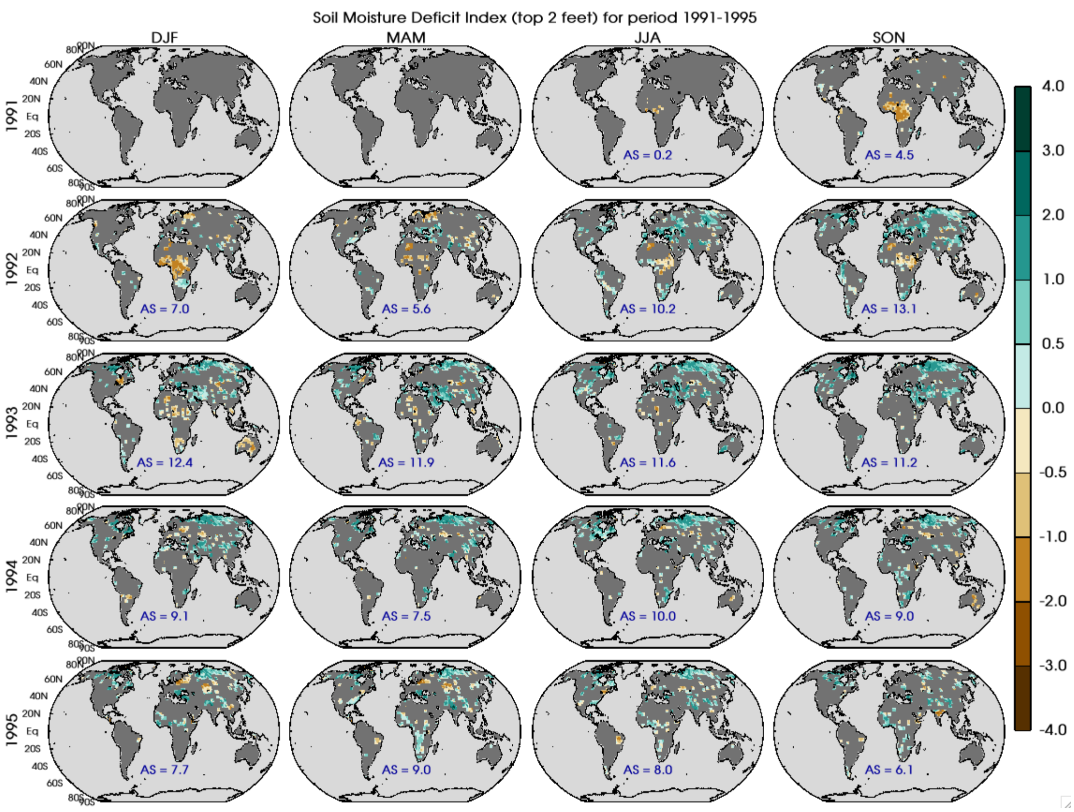


Figure 5. Soil moisture deficit index (SMDI_2) for the top 2 feet of ground depth evaluated seasonally from 1991 to 1995. Grey color is painted over the grid cell where the SMDI_2 is not statistically significant in contrast to counter-factual ensemble. The parameter AS on each panel

mark the percentage of land area which has shown statistically significant dry or wet response after Mt. Pinatubo eruption.

Figure 5 clearly shows that the equatorial region, especially over Africa, has a significant drying response due to Mt. Pinatubo in comparison to long term historical data starting from the SON season of 1991 through the following DJF season. Although less robust, the dryness in this region lasted through MAM of 1993. Severity of drying response reaches up to -2.0 on a scale of extreme wet/dry at 4.0/-4.0, where a severity of – 4.0 reflects the maximum dryness (rarest case) over the entire 1950-2014 calibration period. Figure 4 shows a similar pattern in equatorial African rainfall decrease. Decrease in rainfall was present the first season post Mt. Pinatubo eruption indicating an expected lagged response in SMDI_2. Spatial coherence between these signals is again re-established in the JJA and SON 1992 seasons albeit with more variation in strength of signal.

Meanwhile, in the high latitudes of the northern hemisphere, we see an increase in the store of soil moisture despite a decrease in rainfall in higher latitudes. An exception to this is the Mediterranean (extending towards east Mediterranean and western Asian) region where soil moisture and rainfall, both show an increase during post- Mt. Pinatubo period. This increase in the soil moisture in northern hemisphere is comparatively more pronounced in summer months in comparison to the winter seasons. Thus, despite less water supply through rainfall, there is persistent increase in soil-moisture in the root zone layer starting from JJA season of 1992. This is likely due to less water extracted from this layer through evaporation and transpiration as well as the implemented irrigation in GISS modelE (details in further sections).

Overall, Figure 5 shows equatorial drying signals mostly dominated through the DJF season of the year 1993, but the wet conditions over higher latitudes lasted till 1995. Broadly, 6-

https://doi.org/10.5194/egusphere-2024-2280
Preprint. Discussion started: 3 September 2024


13% of the land region has shown a statistically significance response in terms of dry/wet condition by the end of year 1995 because of the Mt. Pinatubo forcing.

Deeper soil layers approximate longer-term meteorologically defined drought indices better (Narasimhan and Srinivasan 2005). This makes intuitive sense: precipitation provides the recharge for the store of soil moisture and if there is a longer-term decline in precipitation all hydraulically available moisture will be used for plant transpiration (both the deeper stores of water and the soil-penetrating precipitation available) not allowing for deeper depth recharge. Here we evaluate discrete layer depths instead of cumulative depths for two reasons. First, the soil permeability changes with the depth and the inclusion of top layers erroneously reflects the SMDI_2 signal in potentially impermeable regions; second, the SMDI_2 signal gets superposed over the deeper layer response and misleads the actual soil moisture response for the deeper layers.

As expected, when we evaluate the soil moisture deficit response between 2-4 feet soil depth (SMDI_4) in Figure 6, and 4-6-feet soil depth (SMDI_6) in Figure S4, we see similar spatial and temporal distributions as shown in Figure 5 with a corresponding decrease in the percentage of area response. Spatially we see high latitudes across North America and Northeastern and western Asia, equatorial Africa, European, and Mediterranean regions maintain their SMDI-2 trend in Figure 5. However, the total area of response decreases from peak coverages of 12-13% in SMDI-2 to less than 10-12% in SMDI-4 and 7-10% in SMDI_6 (shown in Figure S4). Additional decreases in the degree of impacts are also seen between the three soil layers. Note that the light grey colored regions in Figures 6 and S4 represent regions of impermeability which does affect the total area of response.

https://doi.org/10.5194/egusphere-2024-2280
Preprint. Discussion started: 3 September 2024


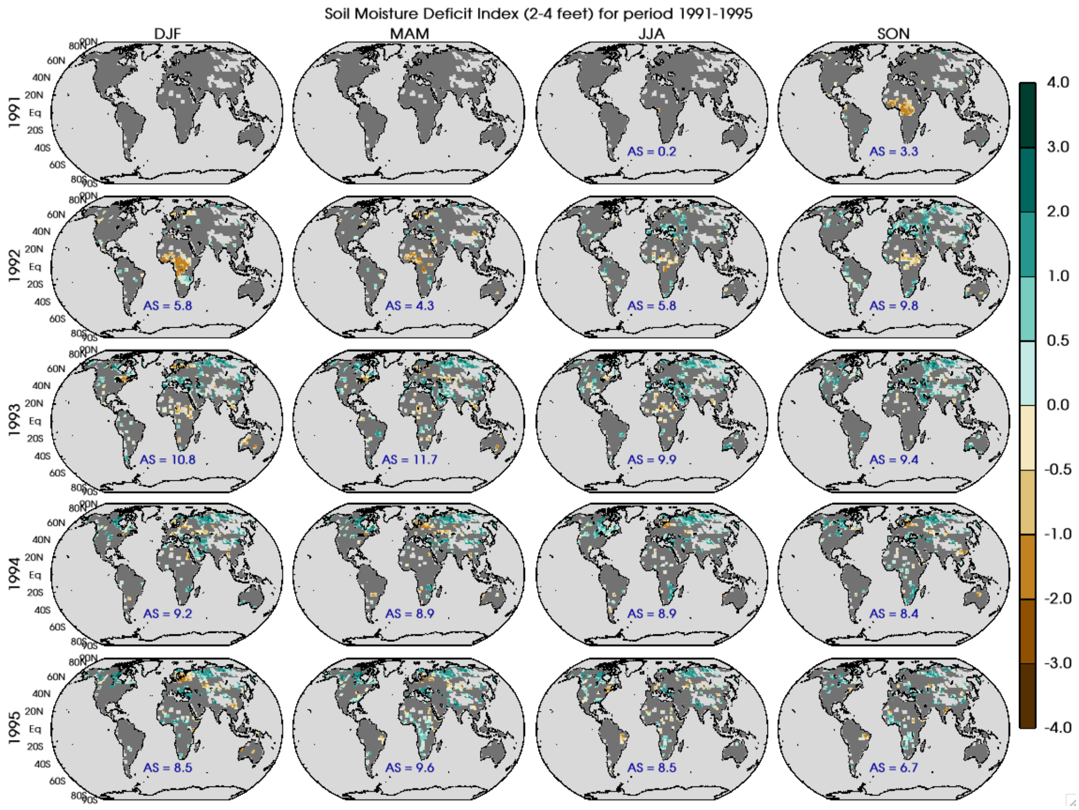


Figure 6. Soil moisture deficit index (SMDI_4) for soil depths between 2-4 feet evaluated seasonally from 1991 to 1995. Grey color is painted over the grid cell where the SMDI_4 is not statistically significant in contrast to counter-factual ensemble. The light grey colored regions represent regions of impermeability. The parameter AS on each panel mark the percentage of land area which has shown statistically significant dry or wet response after Mt. Pinatubo eruption.

### 3.4.2 Seasonal Evapotranspiration Deficit Index (ETDI)

As indicated in the methodology section, ETDI calculation is similar to SMDI but is based on the water stress anomaly which accounts for the difference between actual and potential evapotranspiration. This is a measure of the flux of water between land and atmosphere and like SMDI_2 in Figure 6 it shows robust statistical difference over land.

https://doi.org/10.5194/egusphere-2024-2280
Preprint. Discussion started: 3 September 2024


Figure 7 shows that equatorial decreases in ETDI started developing in the DJF season for the year 1992, and these conditions were persistent over the year. Similar to SMDI_2, ETDI increases over the region encompassing the Mediterranean and western Asia. However, ETDI differs from the SMDI_2 over some of the northern hemisphere regions, especially over Northeastern Asia. A drying response in terms of ETDI in the northern hemisphere regions persisted during 1993 and 1994, whereas SMDI_2 shows an opposite response. This contrasting response in terms of ETDI and SMDI_2 points to the complexity of land-atmosphere interactions over these regions. We utilized model simulated surface energy fluxes (Latent and Sensible heat) to calculate the potential (PET) and actual evapotranspiration (AET) to estimate the water stress ratio. In these regions where soil moisture is available in the summer and early winter months, but a deficit in evapotranspiration reflects the decrease in plant transpiration (latent heat flux), which may be due to the unavailability of plants. Also, the surface temperature (sensible heat flux) response supports the non-water-stressed atmospheric conditions and thus overall, it show a deficit in evapotranspiration. Areas of significant response in terms of ETDI varies from 7 to 14.5% on seasonal basis during the years following the eruption. The largest areas of ETDI coverage occur during the same time periods as SMDI_2 (between JJA 1992 – JJA 1993).

https://doi.org/10.5194/egusphere-2024-2280
Preprint. Discussion started: 3 September 2024


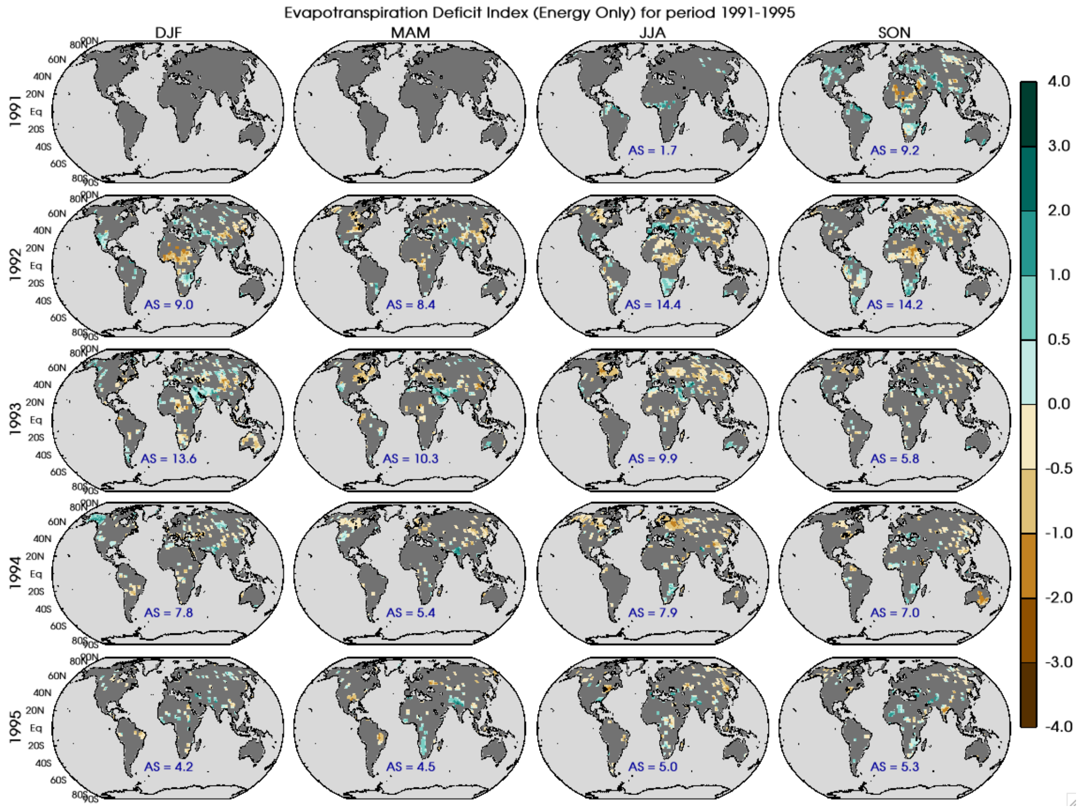


Figure 7. Evapotranspiration deficit index (ETDI) at seasonal scale from 1991 to 1995. Grey color is painted over the grid cell where the ETDI is not statistically significant in contrast to counter-factual ensemble. The parameter AS on each panel mark the percentage of land area which has shown statistically significance dry or wet response after Mt. Pinatubo eruption.

### 3.5 Seasonal Plant Productivity Inferences

SMDI (at depths of 0-2, 2-4, and 4-6 feet) and ETDI have proven helpful in analyzing the climatic impact of the Mt. Pinatubo eruption on a seasonal scale. Additionally, SMDI_2 (top 2 feet) and ETDI have demonstrated elements of a time lag between precipitation on a seasonal scale (Narasimhan and Srinivasan 2005). Crucially, the seasonal depiction of drying/wet conditions via SMDI and ETDI provides a comprehensive overview of prolonged or recurrent

https://doi.org/10.5194/egusphere-2024-2280
Preprint. Discussion started: 3 September 2024


dry/wet conditions in susceptible regions. Moreover, understanding these typical agricultural drought indices indicates potential effects on plant productivity at the seasonal scale.

Broadly the seasonal responses uncovered an interesting behavior in three more deeply explored regions. In equatorial Africa, decreases in both SMDI and ETDI indicated that there was likely a negative impact on plant productivity. On the contrary, the Mediterranean region (encompassing the eastern Mediterranean and western Asian region) showed increases in SMDI and ETDI, indicating a positive effect on plant productivity. Northern Asia, on the other hand, exhibited an increase in SMDI with a decrease in ETDI, indicating that plant productivity likely decreased, but not because of water-based drivers.

### 3.6 High Frequency Impact Pathway Evaluation

Here we use the model output on a daily scale to calculate weekly drought indices in each grid cell. These weekly scale drought indices and changes in other atmospheric variables are explored at the regional scale to understand the associated land-atmosphere interactions in terms of higher-order impacts. High temporal resolution of these parameters is crucial for analysis of different stages of the crop cycle in a region. Considering the complexity of the representation of spatial features, we selected three different regions (shown in Figure 8 and detailed in Table 2) in the northern hemisphere based on the climate response to Mt. Pinatubo in the seasonal analyses presented in Section 3.0.  We followed the same strategy described in Section **2.3.1** to mask out the statistically insignificant grid cells using the counterfactual ensemble after creating the weekly time series for different drought indices and atmospheric parameters.

https://doi.org/10.5194/egusphere-2024-2280
Preprint. Discussion started: 3 September 2024


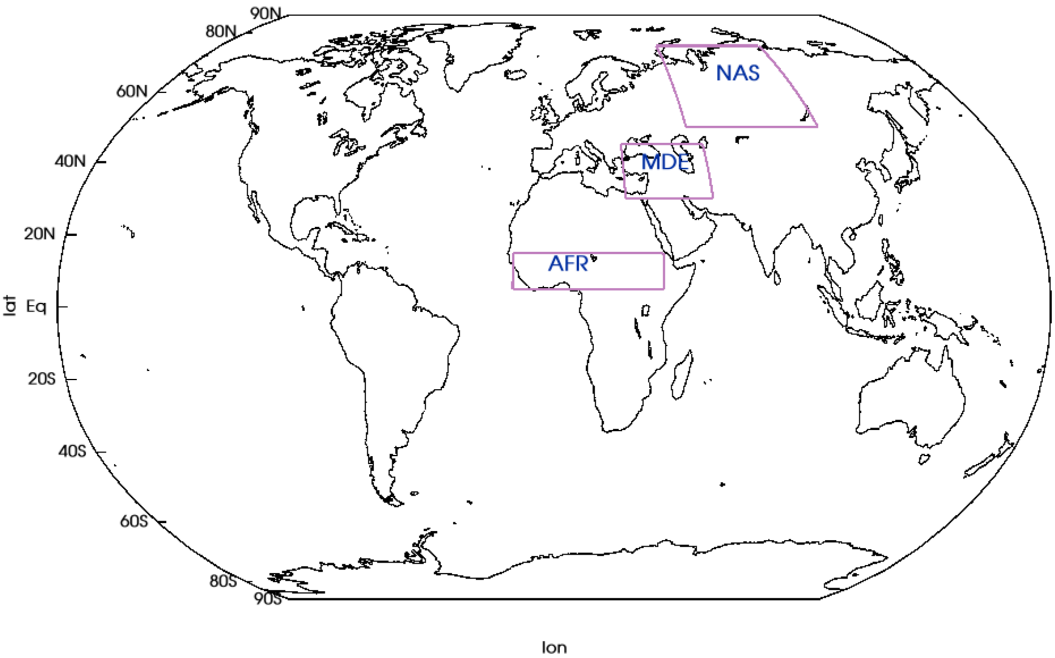


Figure 8: Demarcation of the regions selected over tropics (AFR), mid-latitude (MDE) and high latitudes (NAS) as shown in table 2.

Table 2. Table showing the details of regions demarcated to regional characteristics at a weekly scale.

| Sr No. | Region Name | Region Stamp | Lat boundaries | Lon boundaries |
|---|---|---|---|---|
| 1 | Equatorial Africa Region | AFR | 5° N – 15° N | 15° W - 40° E |
| 2 | Middle East Region | MDE | 30° N - 45° N | 27° E - 60° E |
| 3 | Northern Asia Region | NAS | 50° N - 75° N | 55° E - 110° E |

https://doi.org/10.5194/egusphere-2024-2280
Preprint. Discussion started: 3 September 2024


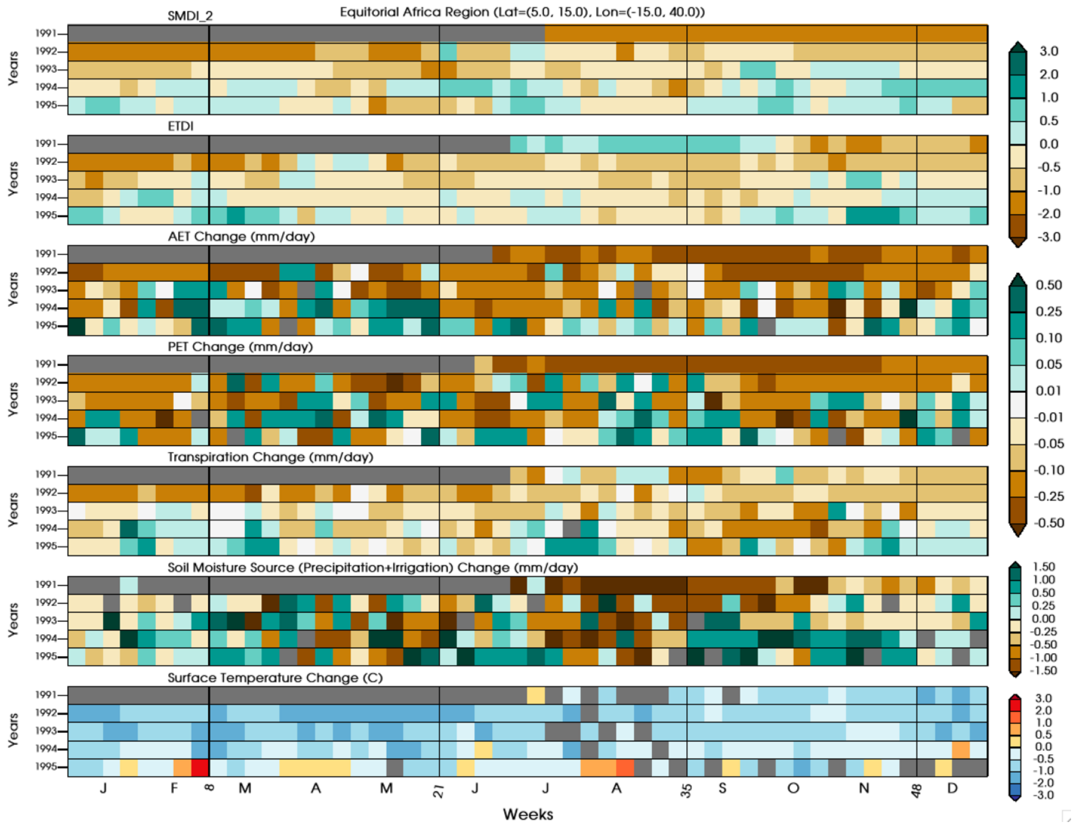


Figure 9. Spatially averaged drought indices (SMDI_2 & ETDI) and anomalies for other drivers (Surface Temperature, Precipitation plus irrigation, Actual and Potential Evapotranspiration, and Transpiration) at weekly scale for the equatorial Africa region (Latitude = 5°-15° N, Longitude = 15° W- 40° E).

### 3.6.1 Equatorial Africa

Figure 9 shows the weekly response to volcanic forcing for the years 1991-1995 in terms of agricultural drought indices (SMDI_2 & ETDI), PET, AET, transpiration, total soil moisture source and surface temperature for an equatorial region in northern Africa. This region exhibits consistent statistical differences across the drivers on a weekly scale and thus the majority of time periods are unmasked revealing the degree of anomaly.

This region lies between the latitude 5-15° N, where the precipitation during the monsoon season shows a decrease in response to a southern migration of the inter-tropical convergence zone in energetically deficit northern hemisphere due to volcanic aerosols preferentially reducing incoming radiation there (Iles et al., 2013; Colose et al., 2016; Singh et al., 2023). Weekly precipitation change in the equatorial African region shows a significant deficit of more than 1.5 mm per day consistently for several weeks, especially during the JJAS monsoon season. This region also shows that a deficit in precipitation during the major precipitation season (JJAS) can result in a soil moisture deficit in the root zone in the following seasons (DJF and MAM in SMDI_2) and consequently affect the entire crop cycle. The root zone soil moisture, SMDI_2, also shows a persistent drying through 1993 and combined with the lack of precipitation, the potential for recharge is limited. Also, this region has no contribution from irrigation as source of additional soil-moisture as shown in figure S5 (bottom panel) (Cook et al., 2020). Cumulative annual rainfall change over this region shows a deficit of 33.2, 9.5 and 3.2 mm per day for the year 1991, 1992 and 1993 and an increase of 10.5 and 13.6 mm per day for the year 1994 and 1995 respectively, where soil-moisture response shows a recovery from the dry conditions.

Hence, it is no surprise that there is a corresponding decrease in ETDI through 1993 that is consistent with this lack of moisture. However, the evaporative demand, as shown by surface temperature change, does not consistently decrease until September of 1991 and hence ETDI is slow to show a decrease in the deficit index. After that point, evaporative demand decreases with lower temperatures contributing to a decrease in ETDI. However, evapotranspiration is dominated by transpiration (Seneviratne et al 2010; Nilson and Assmann 2007 and references therein), and so the majority of the decrease in ETDI is explained by the shown decrease in plant

https://doi.org/10.5194/egusphere-2024-2280
Preprint. Discussion started: 3 September 2024


transpiration. This decrease in plant transpiration is, as expected, well correlated with decreases in AET.

Conclusively, precipitation response in this region shows dominance in regulating the ecohydrological conditions. A substantial decrease in the weekly rainfall over the region perpetuates a root-zone water deficit condition resulting in decreased plant transpiration. Decreases in both SMDI_2 and ETDI thus indicate the developing agricultural drought conditions which are confirmed by a decrease in the direct measure of plant transpiration.

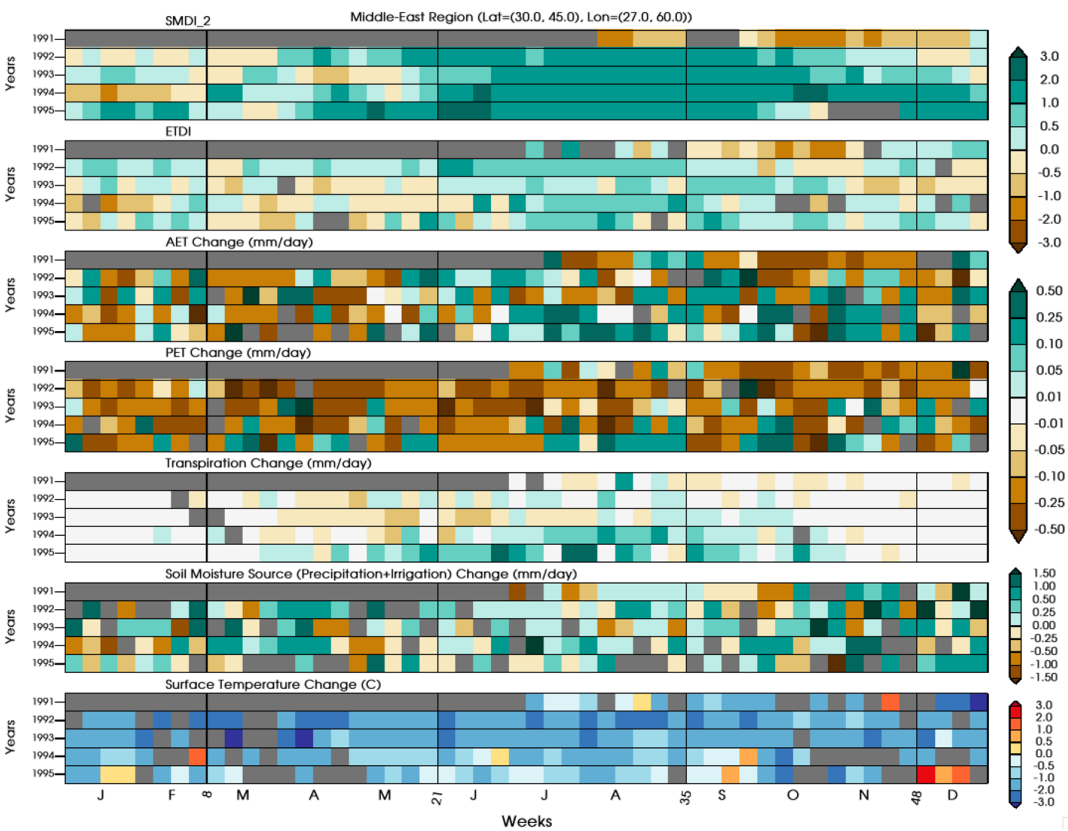


Figure 10. Spatially averaged drought indices (SMDI_2 & ETDI) and anomalies for other drivers (Surface Temperature, Precipitation plus irrigation, Actual and Potential Evapotranspiration, and Transpiration) at weekly scale for Middle East (MDE) Region (Latitude =30° N - 45° N, Longitude=27°-60° E; eastern Mediterranean / western Asian).

https://doi.org/10.5194/egusphere-2024-2280
Preprint. Discussion started: 3 September 2024


### 3.6.2 Middle East Region

Figure 10 shows the region covering the eastern Mediterranean and the western Asian region where rainfall shows a slight increase after the Mt. Pinatubo eruption. Additionally, this region exhibits a significantly positive trend in the irrigation practices post-1050, with a substantial peak over the eastern Mediterranean region following the Mt. Pinatubo eruption (Cook et al., 2020; Figure 1 and 2).

In the eastern Mediterranean, wet and cold autumns and winters persist for several years after the Mt. Pinatubo eruption, offering significant root zone recharge potential. The summer months, in general, reflect a slightly uncertain model response in the regional rainfall with some weeks of deficit and some of excess but an additional supply of water through the irrigation contributes to the overall moisture content in the region (Figure S5). Root zone soil moisture, SMDI_2, shows ample water during the growing seasons through the entire analysis period. Taken together, it is clear that this region is not moisture-limited and there is sufficient precipitation and irrigation supply to recharge root zone moisture as plants grow. Cumulative weekly anomalies show that precipitation change in 1991 is slightly negative (-0.5 mm per day) but an increase in annual rainfall of 13.8, 8.0, 10.9, and 4.5 mm per day is simulated for the year 1992, 1993, 1994 and 1995 respectively. Implemented irrigation over this middle east region shows a strong positive trend for the period 1950-2005 (Cook et al., 2020), and a substantial cumulative increase of 0.5, 1.3, 1.3, 0.8 and 0.9 mm per day in the irrigation for the years 1991 to 1995 serves as the additional source of moisture supply over the region (Cook et al., 2020). Thus, irrigation supplies water especially in summer months when rainfall change shows a few weeks of deficit and contributes 10-20% of the soil-moisture source change (Figure S5).

The corresponding increases in ETDI and AET reflect the ample source of water available for transpiration in the region. Transpiration is again temporally correlated with AET, but the increases are less well pronounced. At the same time, there is a decrease in PET response correlated with the stronger decrease in temperature in this region as compared to equatorial Africa. The decrease in PET coupled with the increase/maintenance in AET (through transpiration) combine to result in increased ETDI. Thus, in general, agricultural productivity is positively affected in this region as there is ample moisture to support it. However, there are still heterogenous patterns in this data showing that 1993, for instance, may have had some impact on plant productivity with positive but lower magnitude ETDI, inconsistent AET, and decreased transpiration.

Regardless of the presence of volcanically induced response or not, the weekly scale analysis demonstrates its importance by virtue of an example from the year 1993, where rainfall deficit is produced during the 15$^{th}$, and 16$^{th}$ weeks (April) of the year. Combined with low SMDI_2, this could result in a lack of moisture availability during a crucial stage of crop cycle. Given the duration, this could significantly influence the overall seasonal crop production. Thus, even if the majority of the crop cycle possess favorable conditions, negative impacts at essential phases of the crop cycle can crucially affect production in ways that seasonal averages would be unable to reveal.

https://doi.org/10.5194/egusphere-2024-2280
Preprint. Discussion started: 3 September 2024


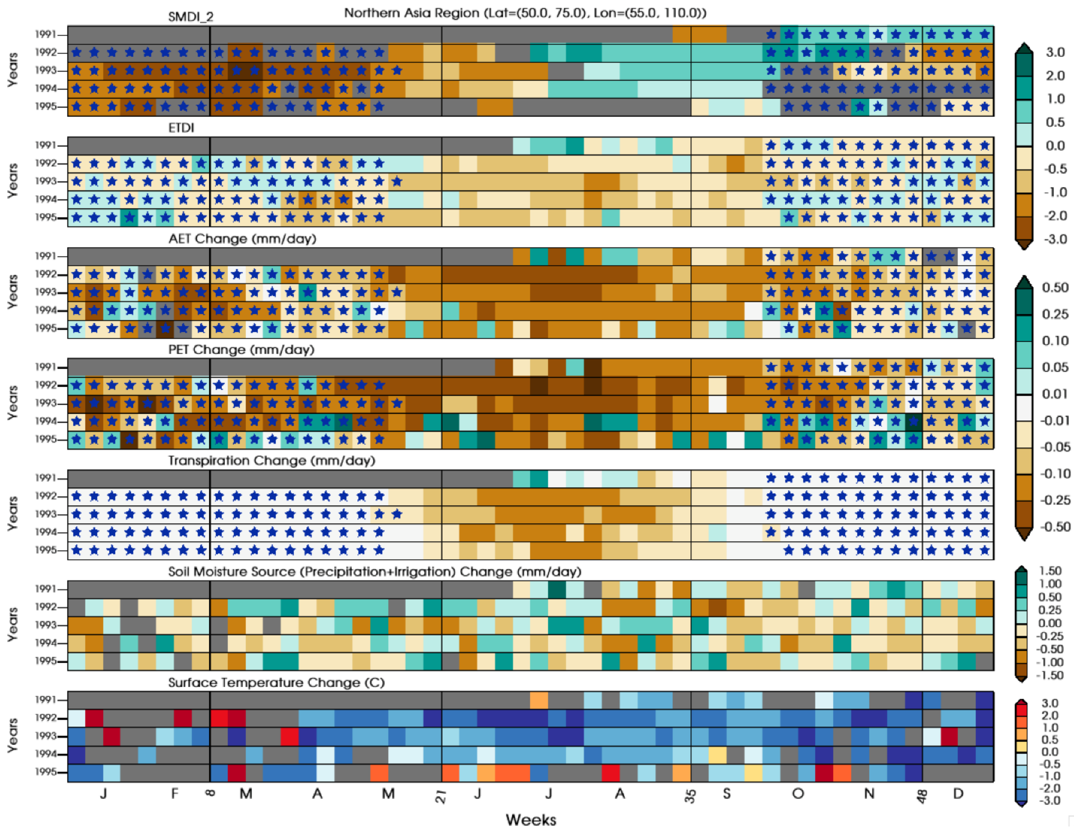


Figure 11. Spatially averaged drought indices (SMDI_2 & ETDI) and anomalies for other drivers (Surface Temperature, Precipitation plus irrigation, Actual and Potential Evapotranspiration, and Transpiration) at weekly scale Northern Asia Region (Latitude =50° N - 75° N, Longitude=55°-110° E). Blue stars represent the weeks with average surface temperature below freezing point.

### 3.6.3 Northern Asia

Finally, we selected a region (NAS) in higher latitudes to explore the interplay between the various drivers governing the conditions for plant productivity. Again, this region exhibits consistent statistical differences across the drivers on a weekly scale. However, with higher latitudes also comes strong seasonal controls over plant productivity with below freezing temperatures, shown with blue stars, halting productivity. Hence our analysis here will focus on months during which plants can grow (~MJJAS).

https://doi.org/10.5194/egusphere-2024-2280
Preprint. Discussion started: 3 September 2024


Precipitation changes are highly uncertain over the entire analysis period, but in general, there is a slight trend towards increased precipitation from Nov 1991- June 1992 followed by decreased precipitation through 1994. As shown in Fig S5, the irrigation contribution to soil moisture in this region is negligible. Cumulative weekly precipitation anomalies show an annual increase of 0.05 mm per day for year 1991 and decrease of -2.0, -4.1, -6.8 and -1.0 mm per day for the years 1992 to 1995 respectively. Alternatively, root zone moisture shows ample water available to plants during the JAS growing months after a strong deficit in the early MJ months. Certainly, in these summer months the melting of frozen surfaces and snow supplies moisture in the upper layers to become wet accounting for this strong dichotomy.

However, there are not corresponding increases in ETDI and AET after the 1991 season. This indicates that even though there is ample water, plants are still not growing; this is conclusively confirmed by the decrease in transpiration starting in 1992. Meanwhile, the simultaneous decrease in PET response is correlated with the strongest decrease in temperature, on the order of 2-3° C, for the three regions.

Unlike the other two regions for which SMDI_2 and ETDI exhibited similar wet/dry patterns, this location shows diverging patterns. Broadly, this reveals that even though there is moisture to support plant productivity, the moisture is not being utilized. Hence, other factors must be the cause of decreased plant transpiration and ETDI. The stronger decrease of PET compared to AET indicates that temperature may be playing a role here. Temperature is a direct proxy of decreased incident radiation. Hence, combined temperature and radiation effects are likely the most important controls on decreased plant productivity in this region, not moisture conditions.

https://doi.org/10.5194/egusphere-2024-2280
Preprint. Discussion started: 3 September 2024


## 4.0 Conclusions

This study has used the Earth system modelling framework to explore the mechanisms by which the 1991 Mt. Pinatubo eruption affected the hydroclimatic conditions and water-based drivers of plant productivity. NASA GISS ModelE2.1 with the interactive chemistry and aerosol microphysical module (MATRIX) has demonstrated a successful simulation of microphysical properties (effective radius of order ~0.5 µm, aerosol extinction of ~0.21) of volcanic aerosol with induced radiative effect of longwave, shortwave, and net forcing of order of +3 $Wm^{-2}$, 8 $Wm^{-2}$ and -5 $Wm^{-2}$ respectively. This is consistent with the observations and other estimates (Russell et al., 1996; Bingen et al., 2004; Stenchikov et al., 1998; Bauman et al., 2003, Lacis et al., 1992, Lacis 2015; Stenchikov et al., 1998; Hansen et al., 1992; Minnis et al., 1993; Brown et al 2024). The temperature response pathway shows Mt. Pinatubo eruption affected global surface cooling by ~0.5 °C with corresponding tropical lower stratosphere warming of 2-3 °C for several years after the eruption. This is consistent with the observations and other modeling estimates (Hansen et al., 1996; Parker et al., 1996; Stenchikov et al., 1998; Minnis et al., 1993; Kirchner et al., 1999; Ramachandran et al., 2000; Dutton and Christy 1992; Brown et al 2024). The GISS model simulates regional patches of decreases in rainfall of the order of 1 mm per day over the tropics and northern hemisphere regions (consistent with Joseph and Zheng, 2011; Liu et al., 2016; Trenberth and Dai, 2007), but the overall response of rainfall is highly uncertain. This study has endeavored to explore the secondary impacts of a volcanic eruption beyond the changes in radiation and temperature by examining agricultural drought indices to better infer impacts to plant productivity. Droughts are among the prime factors affecting regional crop yield at any stage of the crop cycle (Ben Abdelmalek and Nouiri, 2020; Leng and Hall, 2019; Raman et al., 2012). Both SMDI and ETDI represent the developing short- and longer-term conditions

https://doi.org/10.5194/egusphere-2024-2280
Preprint. Discussion started: 3 September 2024


which support plant productivity, especially for agricultural applications. SMDI represents excess/deficit of soil moisture in different layers, whereas ETDI represents the active interaction between the land and atmosphere under perturbed climate conditions. An increase in the gap between the potential evapotranspiration (PET) and actual evapotranspiration (AET) represents the increased water stress condition either by increased potential evapotranspiration (water demand) or by the decrease in water available for evapotranspiration (lower AET). These drought indices confirm the moisture source based dry and wet pattern in early 1992 and the following years over the tropical and northern hemispheres mid-latitude regions correspondingly as a response to the volcanic forcings due to the Mt. Pinatubo eruption. Using both drought indices, we conclude that approximately 10-15% of land region shows statistically significant dry or wet patterns in the volcanically perturbed climate conditions for 1992 and 1993. The fraction of land region showing a significant dry or wet response range between 5-10% for the next two (1994 and 1995) years. Broadly, the seasonal responses uncovered interesting behavior in three regions which we explore more deeply. In equatorial Africa, decreases in both SMDI and ETDI indicated that there was likely a negative impact on plant productivity while in a contrary manner the Middle East region showed increases in SMDI and ETDI indicating a positive impact on plant productivity. Northern Asia in comparison exhibited an increase in SMDI with a decrease in ETDI indicating that plant productivity likely decreased, but not because of water-based drivers.

Using these key pattern differences as motivation, we deepened our analysis of these drought indices using higher temporal (weekly) frequencies and by incorporating AET, PET, and transpiration directly. In general, these regional analyses possess much stronger statistical significance on the weekly scale, and they further confirmed the seasonally based inferences

https://doi.org/10.5194/egusphere-2024-2280
Preprint. Discussion started: 3 September 2024


above. Further, weekly drought indices show the temporal variability characteristics in the signal, which also demonstrates the utility of explaining the effectiveness of short-term dry/wet conditions corresponding to a regional crop cycle. In locations where there is insufficient/excess soil moisture, there is a corresponding decrease/increase in evapotranspiration (AFR/MDE) and hence decreased/increased plant productivity.

This work is the first to conclusively show that there is an excess of root-zone soil moisture in high latitudes (NAS) which is not being utilized by plants to grow establishing the main control is likely temperature and radiation based confirming the results of (Krakauer and Randerson, 2003) and (Dong and Dai, 2017). The intricate nature of the compounded response, particularly regarding the soil moisture-based impact pathways in tropical regions and higher latitudes across the northern hemisphere, also underscores the necessity of broadening the scope of the investigation beyond soil moisture and land-atmosphere interactions. The current setup of the NASA GISS model effectively runs using prescribed vegetation with static plant functional types and leaf area index, and the inclusion of dynamic vegetation could be crucial for adding interactive land surface responses. Also, assessing the influence of the regional and local biome on photosynthesis rate could provide a more detailed understanding of how these processes specifically respond to the climate impact of volcanic forcings. McDermid et al. (2022) have demonstrated the sensitivity of regional hydroclimate to the local changes in soil organic carbon changes using the soil moisture content. The results presented in this study in terms of soil-moisture-based drivers to the plant productivity and surface temperature response in the northern hemisphere high latitudes also hint towards the dominance of temperature effects on enhanced carbon sink in terms of soil and plant respiration and reduced NPP (Krakauer and Randerson, 2003; Lucht et al., 2002). Meanwhile, water-based drivers dominate productivity responses in

https://doi.org/10.5194/egusphere-2024-2280
Preprint. Discussion started: 3 September 2024


multiple tropical and sub-tropical regions. Our results illustrate that soil-moisture-based conditions in the different regions can be useful for evaluating and understanding the full impacts on the agricultural yield and regional carbon sink response if the dynamic vegetation and crop cover changes. A recently developed fully demographic dynamic vegetation model (ModelE-BiomE v.1.0 (Weng et al., 2022)) with interactive biophysical and biogeochemical feedback between climate and land systems for NASA GISS ModelE could be helpful in evaluating the carbon cycle response under such forcings.

**Code/Data availability.**

Details to support the results in the manuscript is available as supplementary information is provided with the manuscript. GISS Model code snapshots are available at https://simplex.giss.nasa.gov/snapshots/ (National Aeronautics and Space Administration, 2024) and calculated diagnostics are available at zenodo repository (https://zenodo.org/records/12734905) (Singh et al., 2024). However, raw model output and data at high temporal (daily) resolution and codes are available on request from author due to large data volume.

**Acknowledgements**

Resources supporting this work were provided by the NASA High-End Computing (HEC) Program through the NASA Center for Climate Simulation (NCCS) at Goddard Space Flight Center. The authors thank Ben I Cook, Nancy Y Kiang, Igor Aleinov and Michael Puma for their input through multiple discussions with the project members. RS, KT, DB, LS, BW, and KM were supported by the Laboratory Directed Research and Development program at Sandia National Laboratories, a multi-mission laboratory managed and operated by National Technology and Engineering Solutions of Sandia LLC, a wholly owned subsidiary of Honeywell International Inc. for the U.S. Department of Energy's National Nuclear Security Administration under contract DE-NA0003525. This paper describes objective technical results and analysis. Any subjective views or opinions that might be expressed in the paper do not necessarily represent the views of the U.S. Department of Energy or the United States Government.

**Author's contributions**

RS, KT, DB, LS and KM identified the study period in consultation with the other authors and RS, KT, DB, LS and BW designed the underlying simulations strategies. RS and KT implemented it and performed the simulations using NASA GISS ModelE. RS and KT have performed the analysis. RS created the figures in close collaboration with all authors. RS wrote the first draft of the manuscript, and all other authors has contributed the writing of subsequent drafts. All authors contributed to the interpretation of results.

**Competing interests**

One of the co-authors is member of the editorial board of Atmospheric Chemistry and Physics.

**Short Summary**

Analysis of post-eruption climate conditions using the impact metrics is crucial for understanding the hydroclimatic responses. We used NASA's Earth system model to perform the experiments and utilize the moisture-based impact metrics and hydrological variables to investigate the effect of volcanically induced conditions that govern plant productivity. This study demonstrates the Mt. Pinatubo's impact on drivers of plant productivity and regional and seasonal dependence of different drivers.

**Reference:**

Allen, R.G., Pereira, L.S., Raes, D., et al. (1998) Crop Evapotranspiration-Guidelines for Computing Crop Water Requirements-FAO Irrigation and Drainage Paper 56. FAO, Rome, 300(9): D05109.

Aquila, V., Oman, L. D., Stolarski, R. S., Colarco, P. R., and Newman, P. A.: Dispersion of the volcanic sulfate cloud from a Mount Pinatubo–like eruption, Journal of Geophysical Research: Atmospheres, 117, https://doi.org/10.1029/2011JD016968, 2012.

Barnes, E. A., Solomon, S., and Polvani, L. M.: Robust Wind and Precipitation Responses to the Mount Pinatubo Eruption, as Simulated in the CMIP5 Models, Journal of Climate, 29, 4763–4778, https://doi.org/10.1175/JCLI-D-15-0658.1, 2016.

Barnes, J. E. and Hofmann, D. J.: Lidar measurements of stratospheric aerosol over Mauna Loa Observatory, Geophysical Research Letters, 24, 1923–1926, https://doi.org/10.1029/97GL01943, 1997.

Bauer, S. E., Wright, D. L., Koch, D., Lewis, E. R., McGraw, R., Chang, L.-S., Schwartz, S. E., and Ruedy, R.: MATRIX (Multiconfiguration Aerosol TRacker of mIXing state): an aerosol microphysical module for global atmospheric models, Atmospheric Chemistry and Physics, 8, 6003–6035, https://doi.org/10.5194/acp-8-6003-2008, 2008.

https://doi.org/10.5194/egusphere-2024-2280
Preprint. Discussion started: 3 September 2024


Bauer, S. E., Ault, A., and Prather, K. A.: Evaluation of aerosol mixing state classes in the GISS modelE-MATRIX climate model using single-particle mass spectrometry measurements, Journal of Geophysical Research: Atmospheres, 118, 9834–9844, https://doi.org/10.1002/jgrd.50700, 2013.

Bauer, S. E., Tsigaridis, K., Faluvegi, G., Kelley, M., Lo, K. K., Miller, R. L., Nazarenko, L., Schmidt, G. A., and Wu, J.: Historical (1850–2014) Aerosol Evolution and Role on Climate Forcing Using the GISS ModelE2.1 Contribution to CMIP6, Journal of Advances in Modeling Earth Systems, 12, e2019MS001978, https://doi.org/10.1029/2019MS001978, 2020.

Bauman, J. J., Russell, P. B., Geller, M. A., and Hamill, P.: A stratospheric aerosol climatology from SAGE II and CLAES measurements: 2. Results and comparisons, 1984–1999, Journal of Geophysical Research: Atmospheres, 108, https://doi.org/10.1029/2002JD002993, 2003.

Bekki, S.: Oxidation of volcanic SO2: A sink for stratospheric OH and H2O, Geophysical Research Letters, 22, 913–916, https://doi.org/10.1029/95GL00534, 1995.

Ben Abdelmalek, M. and Nouiri, I.: Study of trends and mapping of drought events in Tunisia and their impacts on agricultural production, Science of The Total Environment, 734, 139311, https://doi.org/10.1016/j.scitotenv.2020.139311, 2020.

Bingen, C., Fussen, D., and Vanhellemont, F.: A global climatology of stratospheric aerosol size distribution parameters derived from SAGE II data over the period 1984–2000: 1. Methodology and climatological observations, Journal of Geophysical Research: Atmospheres, 109, https://doi.org/10.1029/2003JD003518, 2004.

Bluth, G. J. S., Doiron, S. D., Schnetzler, C. C., Krueger, A. J., and Walter, L. S.: Global tracking of the SO2 clouds from the June, 1991 Mount Pinatubo eruptions, Geophysical Research Letters, 19, 151–154, https://doi.org/10.1029/91GL02792, 1992.

Brad Adams, J., Mann, M. E., and Ammann, C. M.: Proxy evidence for an El Niño-like response to volcanic forcing, Nature, 426, 274–278, https://doi.org/10.1038/nature02101, 2003.

Briffa, K. R., Jones, P. D., Schweingruber, F. H., and Osborn, T. J.: Influence of volcanic eruptions on Northern Hemisphere summer temperature over the past 600 years, Nature, 393, 450–455, https://doi.org/10.1038/30943, 1998.

Brown, H. Y., Wagman, B., Bull, D., Peterson, K., Hillman, B., Liu, X., Ke, Z., and Lin, L.: Validating a microphysical prognostic stratospheric aerosol implementation in E3SMv2 using the Mount Pinatubo eruption, EGUsphere, 1–46, https://doi.org/10.5194/egusphere-2023-3041, 2024.

Carn, S. A., Fioletov, V. E., McLinden, C. A., Li, C., and Krotkov, N. A.: A decade of global volcanic SO2 emissions measured from space, Sci Rep, 7, 44095, https://doi.org/10.1038/srep44095, 2017.

https://doi.org/10.5194/egusphere-2024-2280
Preprint. Discussion started: 3 September 2024


Chen, D.-X. and Coughenour, M. B.: Photosynthesis, transpiration, and primary productivity: Scaling up from leaves to canopies and regions using process models and remotely sensed data, Global Biogeochemical Cycles, 18, https://doi.org/10.1029/2002GB001979, 2004.

Colose, C. M., LeGrande, A. N., and Vuille, M.: Hemispherically asymmetric volcanic forcing of tropical hydroclimate during the last millennium, Earth System Dynamics, 7, 681–696, https://doi.org/10.5194/esd-7-681-2016, 2016.

Cook, B. I., McDermid, S. S., Puma, M. J., Williams, A. P., Seager, R., Kelley, M., Nazarenko, L., and Aleinov, I.: Divergent Regional Climate Consequences of Maintaining Current Irrigation Rates in the 21st Century, Journal of Geophysical Research: Atmospheres, 125, e2019JD031814, https://doi.org/10.1029/2019JD031814, 2020.

Denissen, J. M. C., Teuling, A. J., Pitman, A. J., Koirala, S., Migliavacca, M., Li, W., Reichstein, M., Winkler, A. J., Zhan, C., and Orth, R.: Widespread shift from ecosystem energy to water limitation with climate change, Nat. Clim. Chang., 12, 677–684, https://doi.org/10.1038/s41558-022-01403-8, 2022.

Deshler, T., Hervig, M. E., Hofmann, D. J., Rosen, J. M., and Liley, J. B.: Thirty years of in situ stratospheric aerosol size distribution measurements from Laramie, Wyoming (41°N), using balloon-borne instruments, Journal of Geophysical Research: Atmospheres, 108, https://doi.org/10.1029/2002JD002514, 2003.

Dhomse, S. S., Emmerson, K. M., Mann, G. W., Bellouin, N., Carslaw, K. S., Chipperfield, M. P., Hommel, R., Abraham, N. L., Telford, P., Braesicke, P., Dalvi, M., Johnson, C. E., O'Connor, F., Morgenstern, O., Pyle, J. A., Deshler, T., Zawodny, J. M., and Thomason, L. W.: Aerosol microphysics simulations of the Mt.~Pinatubo eruption with the UM-UKCA composition-climate model, Atmospheric Chemistry and Physics, 14, 11221–11246, https://doi.org/10.5194/acp-14-11221-2014, 2014.

Dong, B. and Dai, A.: The uncertainties and causes of the recent changes in global evapotranspiration from 1982 to 2010, Clim Dyn, 49, 279–296, https://doi.org/10.1007/s00382-016-3342-x, 2017.

Dutton, E. G. and Christy, J. R.: Solar radiative forcing at selected locations and evidence for global lower tropospheric cooling following the eruptions of El Chichón and Pinatubo, Geophysical Research Letters, 19, 2313–2316, https://doi.org/10.1029/92GL02495, 1992.

English, J. M., Toon, O. B., and Mills, M. J.: Microphysical simulations of large volcanic eruptions: Pinatubo and Toba, Journal of Geophysical Research: Atmospheres, 118, 1880–1895, https://doi.org/10.1002/jgrd.50196, 2013.

Farquhar, G. D. and Roderick, M. L.: Pinatubo, Diffuse Light, and the Carbon Cycle, Science, 299, 1997–1998, https://doi.org/10.1126/science.1080681, 2003.

Fujiwara, M., Martineau, P., and Wright, J. S.: Surface temperature response to the major volcanic eruptions in multiple reanalysis data sets, Atmospheric Chemistry and Physics, 20, 345–374, https://doi.org/10.5194/acp-20-345-2020, 2020.

Gao, C. Y., Naik, V., Horowitz, L. W., Ginoux, P., Paulot, F., Dunne, J., Mills, M., Aquila, V., and Colarco, P.: Volcanic Drivers of Stratospheric Sulfur in GFDL ESM4, Journal of Advances in Modeling Earth Systems, 15, e2022MS003532, https://doi.org/10.1029/2022MS003532, 2023.

Gao, F., Morisette, J. T., Wolfe, R. E., Ederer, G., Pedelty, J., Masuoka, E., Myneni, R., Tan, B., and Nightingale, J.: An Algorithm to Produce Temporally and Spatially Continuous MODIS-LAI Time Series, IEEE Geoscience and Remote Sensing Letters, 5, 60–64, https://doi.org/10.1109/LGRS.2007.907971, 2008.

Gery, M. W., Whitten, G. Z., Killus, J. P., and Dodge, M. C.: A photochemical kinetics mechanism for urban and regional scale computer modeling, Journal of Geophysical Research: Atmospheres, 94, 12925–12956, https://doi.org/10.1029/JD094iD10p12925, 1989.

Gu, G. and Adler, R. F.: Precipitation and Temperature Variations on the Interannual Time Scale: Assessing the Impact of ENSO and Volcanic Eruptions, Journal of Climate, 24, 2258–2270, https://doi.org/10.1175/2010JCLI3727.1, 2011.

Gu, G. and Adler, R. F.: Large-scale, inter-annual relations among surface temperature, water vapour and precipitation with and without ENSO and volcano forcings, International Journal of Climatology, 32, 1782–1791, https://doi.org/10.1002/joc.2393, 2012.

Gu, G., Adler, R. F., Huffman, G. J., and Curtis, S.: Tropical Rainfall Variability on Interannual-to-Interdecadal and Longer Time Scales Derived from the GPCP Monthly Product, Journal of Climate, 20, 4033–4046, https://doi.org/10.1175/JCLI4227.1, 2007.

Gu, L., Baldocchi, D., Verma, S. B., Black, T. A., Vesala, T., Falge, E. M., and Dowty, P. R.: Advantages of diffuse radiation for terrestrial ecosystem productivity, Journal of Geophysical Research: Atmospheres, 107, ACL 2-1-ACL 2-23, https://doi.org/10.1029/2001JD001242, 2002.

Gu, L., Baldocchi, D. D., Wofsy, S. C., Munger, J. W., Michalsky, J. J., Urbanski, S. P., and Boden, T. A.: Response of a Deciduous Forest to the Mount Pinatubo Eruption: Enhanced Photosynthesis, Science, 299, 2035–2038, https://doi.org/10.1126/science.1078366, 2003.

Hane, D. C. and Pumphrey, F. V.: Yield-evapotranspiration relationships and seasonal crop coefficients for frequently irrigated potatoes, American Potato Journal, 61, 661–668, https://doi.org/10.1007/BF02852929, 1984.

Hansen, J., Lacis, A., Ruedy, R., and Sato, M.: Potential climate impact of Mount Pinatubo eruption, Geophysical Research Letters, 19, 215–218, https://doi.org/10.1029/91GL02788, 1992.

https://doi.org/10.5194/egusphere-2024-2280
Preprint. Discussion started: 3 September 2024


Hansen, J., Sato, M., Ruedy, R., Lacis, A., Asamoah, K., Borenstein, S., Brown, E., Cairns, B., Caliri, G., Campbell, M., Curran, B., de Castro, S., Druyan, L., Fox, M., Johnson, C., Lerner, J., McCormick, M. P., Miller, R., Minnis, P., Morrison, A., Pandolfo, L., Ramberrann, I., Zaucker, F., Robinson, M., Russell, P., Shah, K., Stone, P., Tegen, I., Thomason, L., Wilder, J., and Wilson, H.: A Pinatubo Climate Modeling Investigation, in: The Mount Pinatubo Eruption, Berlin, Heidelberg, 233–272, https://doi.org/10.1007/978-3-642-61173-5_20, 1996.

Hansen, J. E., Lacis, A. A., Lee, P., and Wang, W.-C.: Climatic Effects of Atmospheric Aerosols, Annals of the New York Academy of Sciences, 338, 575–587, https://doi.org/10.1111/j.1749-6632.1980.tb17151.x, 1980.

Hao, Z., Xiong, D., Zheng, J., Yang, L. E., and Ge, Q.: Volcanic eruptions, successive poor harvests and social resilience over southwest China during the 18–19th century, Environ. Res. Lett., 15, 105011, https://doi.org/10.1088/1748-9326/abb159, 2020.

Hitchman, M. H., McKay, M., and Trepte, C. R.: A climatology of stratospheric aerosol, J. Geophys. Res.-Atmos., 99, 20689–20700, https://doi.org/10.1029/94JD01525, 1994.

Hoesly, R. M., Smith, S. J., Feng, L., Klimont, Z., Janssens-Maenhout, G., Pitkanen, T., Seibert, J. J., Vu, L., Andres, R. J., Bolt, R. M., Bond, T. C., Dawidowski, L., Kholod, N., Kurokawa, J., Li, M., Liu, L., Lu, Z., Moura, M. C. P., O'Rourke, P. R., and Zhang, Q.: Historical (1750–2014) anthropogenic emissions of reactive gases and aerosols from the Community Emissions Data System (CEDS), Geoscientific Model Development, 11, 369–408, https://doi.org/10.5194/gmd-11-369-2018, 2018.

Huhtamaa, H. and Helama, S.: Distant impact: tropical volcanic eruptions and climate-driven agricultural crises in seventeenth-century Ostrobothnia, Finland, Journal of Historical Geography, 57, 40–51, https://doi.org/10.1016/j.jhg.2017.05.011, 2017.

Iles, C. E., Hegerl, G. C., Schurer, A. P., and Zhang, X.: The effect of volcanic eruptions on global precipitation, Journal of Geophysical Research: Atmospheres, 118, 8770–8786, https://doi.org/10.1002/jgrd.50678, 2013.

Ito, G., Romanou, A., Kiang, N. Y., Faluvegi, G., Aleinov, I., Ruedy, R., Russell, G., Lerner, P., Kelley, M., and Lo, K.: Global Carbon Cycle and Climate Feedbacks in the NASA GISS ModelE2.1, Journal of Advances in Modeling Earth Systems, 12, e2019MS002030, https://doi.org/10.1029/2019MS002030, 2020.

Jones, C. D. and Cox, P. M.: Modeling the volcanic signal in the atmospheric CO2 record, Global Biogeochemical Cycles, 15, 453–465, https://doi.org/10.1029/2000GB001281, 2001.

Joseph, R. and Zeng, N.: Seasonally Modulated Tropical Drought Induced by Volcanic Aerosol, Journal of Climate, 24, 2045–2060, https://doi.org/10.1175/2009JCLI3170.1, 2011.

https://doi.org/10.5194/egusphere-2024-2280
Preprint. Discussion started: 3 September 2024



Kelley, M., Schmidt, G. A., Nazarenko, L. S., Bauer, S. E., Ruedy, R., Russell, G. L., Ackerman, A. S., Aleinov, I., Bauer, M., Bleck, R., Canuto, V., Cesana, G., Cheng, Y., Clune, T. L., Cook, B. I., Cruz, C. A., Del Genio, A. D., Elsaesser, G. S., Faluvegi, G., Kiang, N. Y., Kim, D., Lacis, A. A., Leboissetier, A., LeGrande, A. N., Lo, K. K., Marshall, J., Matthews, E. E., McDermid, S., Mezuman, K., Miller, R. L., Murray, L. T., Oinas, V., Orbe, C., García-Pando, C. P., Perlwitz, J. P., Puma, M. J., Rind, D., Romanou, A., Shindell, D. T., Sun, S., Tausnev, N., Tsigaridis, K., Tselioudis, G., Weng, E., Wu, J., and Yao, M.-S.: GISS-E2.1: Configurations and Climatology, Journal of Advances in Modeling Earth Systems, 12, e2019MS002025, https://doi.org/10.1029/2019MS002025, 2020.

Keshavarz, M. R., Vazifedoust, M., and Alizadeh, A.: Drought monitoring using a Soil Wetness Deficit Index (SWDI) derived from MODIS satellite data, Agricultural Water Management, 132, 37–45, https://doi.org/10.1016/j.agwat.2013.10.004, 2014.

Kiehl, J. T. and Trenberth, K. E.: Earth's Annual Global Mean Energy Budget, Bulletin of the American Meteorological Society, 78, 197–208, https://doi.org/10.1175/1520-0477(1997)078<0197:EAGMEB>2.0.CO;2, 1997.

Kim, Y., Moorcroft, P. R., Aleinov, I., Puma, M. J., and Kiang, N. Y.: Variability of phenology and fluxes of water and carbon with observed and simulated soil moisture in the Ent Terrestrial Biosphere Model (Ent TBM version 1.0.1.0.0), Geoscientific Model Development, 8, 3837–3865, https://doi.org/10.5194/gmd-8-3837-2015, 2015.

Kinne, S., Toon, O. B., and Prather, M. J.: Buffering of stratospheric circulation by changing amounts of tropical ozone - a Pinatubo case study, Geophysical Research Letters (American Geophysical Union); (United States), 19:19, https://doi.org/10.1029/92GL01937, 1992.

Krakauer, N. Y. and Randerson, J. T.: Do volcanic eruptions enhance or diminish net primary production? Evidence from tree rings, Global Biogeochemical Cycles, 17, https://doi.org/10.1029/2003GB002076, 2003.

Labitzke, K. and McCormick, M. P.: Stratospheric temperature increases due to Pinatubo aerosols, Geophysical Research Letters, 19, 207–210, https://doi.org/10.1029/91GL02940, 1992.

Lacis, A.: Volcanic aerosol radiative properties, PAGES Mag, 23, 50–51, https://doi.org/10.22498/pages.23.2.50, 2015.

Lacis, A., Hansen, J., and Sato, M.: Climate forcing by stratospheric aerosols, Geophysical Research Letters, 19, 1607–1610, https://doi.org/10.1029/92GL01620, 1992.

Lacis, A. A. and Hansen, J.: A Parameterization for the Absorption of Solar Radiation in the Earth's Atmosphere, Journal of the Atmospheric Sciences, 31, 118–133, https://doi.org/10.1175/1520-0469(1974)031<0118:APFTAO>2.0.CO;2, 1974.

https://doi.org/10.5194/egusphere-2024-2280
Preprint. Discussion started: 3 September 2024


Lambert, A., Grainger, R. G., Remedios, J. J., Rodgers, C. D., Corney, M., and Taylor, F. W.: Measurements of the evolution of the Mt. Pinatubo aerosol cloud by ISAMS, Geophysical Research Letters, 20, 1287–1290, https://doi.org/10.1029/93GL00827, 1993.

LeGrande, A. N. and Anchukaitis, K. J.: Volcanic eruptions and climate, 23, 2015.

LeGrande, A. N., Tsigaridis, K., and Bauer, S. E.: Role of atmospheric chemistry in the climate impacts of stratospheric volcanic injections, Nature Geosci, 9, 652–655, https://doi.org/10.1038/ngeo2771, 2016.

Leng, G. and Hall, J.: Crop yield sensitivity of global major agricultural countries to droughts and the projected changes in the future, Science of The Total Environment, 654, 811–821, https://doi.org/10.1016/j.scitotenv.2018.10.434, 2019.

Li, J., Xie, S.-P., Cook, E. R., Morales, M. S., Christie, D. A., Johnson, N. C., Chen, F., D'Arrigo, R., Fowler, A. M., Gou, X., and Fang, K.: El Niño modulations over the past seven centuries, Nature Clim Change, 3, 822–826, https://doi.org/10.1038/nclimate1936, 2013.

Liu, F., Chai, J., Wang, B., Liu, J., Zhang, X., and Wang, Z.: Global monsoon precipitation responses to large volcanic eruptions, Sci Rep, 6, 24331, https://doi.org/10.1038/srep24331, 2016.

Lobell, D. B. and Field, C. B.: Global scale climate–crop yield relationships and the impacts of recent warming, Environ. Res. Lett., 2, 014002, https://doi.org/10.1088/1748-9326/2/1/014002, 2007.

Lucht, W., Prentice, I. C., Myneni, R. B., Sitch, S., Friedlingstein, P., Cramer, W., Bousquet, P., Buermann, W., and Smith, B.: Climatic Control of the High-Latitude Vegetation Greening Trend and Pinatubo Effect, Science, 296, 1687–1689, https://doi.org/10.1126/science.1071828, 2002.

Manning, J. G., Ludlow, F., Stine, A. R., Boos, W. R., Sigl, M., and Marlon, J. R.: Volcanic suppression of Nile summer flooding triggers revolt and constrains interstate conflict in ancient Egypt, Nat Commun, 8, 900, https://doi.org/10.1038/s41467-017-00957-y, 2017.

van Marle, M. J. E., Kloster, S., Magi, B. I., Marlon, J. R., Daniau, A.-L., Field, R. D., Arneth, A., Forrest, M., Hantson, S., Kehrwald, N. M., Knorr, W., Lasslop, G., Li, F., Mangeon, S., Yue, C., Kaiser, J. W., and van der Werf, G. R.: Historic global biomass burning emissions for CMIP6 (BB4CMIP) based on merging satellite observations with proxies and fire models (1750–2015), Geoscientific Model Development, 10, 3329–3357, https://doi.org/10.5194/gmd-10-3329-2017, 2017.

McCormick, M. P. and Veiga, R. E.: SAGE II measurements of early Pinatubo aerosols, Geophysical Research Letters, 19, 155–158, https://doi.org/10.1029/91GL02790, 1992.

McCormick, M. P., Thomason, L. W., and Trepte, C. R.: Atmospheric effects of the Mt Pinatubo eruption, Nature, 373, 399–404, https://doi.org/10.1038/373399a0, 1995.

https://doi.org/10.5194/egusphere-2024-2280
Preprint. Discussion started: 3 September 2024


McDermid, S. S., Montes, C., Cook, B. I., Puma, M. J., Kiang, N. Y., and Aleinov, I.: The Sensitivity of Land–Atmosphere Coupling to Modern Agriculture in the Northern Midlatitudes, Journal of Climate, 32, 465–484, https://doi.org/10.1175/JCLI-D-17-0799.1, 2019.

McDermid, S. S., Weng, E., Puma, M., Cook, B., Hengl, T., Sanderman, J., Lannoy, G. J. M. D., and Aleinov, I.: Soil Carbon Losses Reduce Soil Moisture in Global Climate Model Simulations, Earth Interactions, 26, 195–208, https://doi.org/10.1175/EI-D-22-0003.1, 2022.

McGraw, Z., DallaSanta, K., Polvani, L. M., Tsigaridis, K., Orbe, C., and Bauer, S. E.: Severe Global Cooling After Volcanic Super-Eruptions? The Answer Hinges on Unknown Aerosol Size, Journal of Climate, 37, 1449–1464, https://doi.org/10.1175/JCLI-D-23-0116.1, 2024.

McKee, T. B., Doesken, N. J., and Kleist, J.: THE RELATIONSHIP OF DROUGHT FREQUENCY AND DURATION TO TIME SCALES, n.d.

Miller, R. L., Cakmur, R. V., Perlwitz, J., Geogdzhayev, I. V., Ginoux, P., Koch, D., Kohfeld, K. E., Prigent, C., Ruedy, R., Schmidt, G. A., and Tegen, I.: Mineral dust aerosols in the NASA Goddard Institute for Space Sciences ModelE atmospheric general circulation model, Journal of Geophysical Research: Atmospheres, 111, https://doi.org/10.1029/2005JD005796, 2006.

Mills, M. J., Schmidt, A., Easter, R., Solomon, S., Kinnison, D. E., Ghan, S. J., Neely III, R. R., Marsh, D. R., Conley, A., Bardeen, C. G., and Gettelman, A.: Global volcanic aerosol properties derived from emissions, 1990–2014, using CESM1(WACCM), Journal of Geophysical Research: Atmospheres, 121, 2332–2348, https://doi.org/10.1002/2015JD024290, 2016.

Milly, P. C. D. and Dunne, K. A.: Potential evapotranspiration and continental drying, Nature Clim Change, 6, 946–949, https://doi.org/10.1038/nclimate3046, 2016.

Minnis, P., Harrison, E. F., Stowe, L. L., Gibson, G. G., Denn, F. M., Doelling, D. R., and Smith, W. L.: Radiative Climate Forcing by the Mount Pinatubo Eruption, Science, 259, 1411–1415, https://doi.org/10.1126/science.259.5100.1411, 1993.

Mullapudi, A., Vibhute, A. D., Mali, S., and Patil, C. H.: A review of agricultural drought assessment with remote sensing data: methods, issues, challenges and opportunities, Appl Geomat, 15, 1–13, https://doi.org/10.1007/s12518-022-00484-6, 2023.

Myneni, R. B., Hoffman, S., Knyazikhin, Y., Privette, J. L., Glassy, J., Tian, Y., Wang, Y., Song, X., Zhang, Y., Smith, G. R., Lotsch, A., Friedl, M., Morisette, J. T., Votava, P., Nemani, R. R., and Running, S. W.: Global products of vegetation leaf area and fraction absorbed PAR from year one of MODIS data, Remote Sensing of Environment, 83, 214–231, https://doi.org/10.1016/S0034-4257(02)00074-3, 2002.

Narasimhan, B. and Srinivasan, R.: Development and evaluation of Soil Moisture Deficit Index (SMDI) and Evapotranspiration Deficit Index (ETDI) for agricultural drought monitoring, Agricultural and Forest Meteorology, 133, 69–88, https://doi.org/10.1016/j.agrformet.2005.07.012, 2005.

https://doi.org/10.5194/egusphere-2024-2280
Preprint. Discussion started: 3 September 2024


Nilson, S. E. and Assmann, S. M.: The Control of Transpiration. Insights from Arabidopsis, Plant Physiol, 143, 19–27, https://doi.org/10.1104/pp.106.093161, 2007.

Olesen, J. E. and Bindi, M.: Consequences of climate change for European agricultural productivity, land use and policy, European Journal of Agronomy, 16, 239–262, https://doi.org/10.1016/S1161-0301(02)00004-7, 2002.

Paik, S., Min, S.-K., Iles, C. E., Fischer, E. M., and Schurer, A. P.: Volcanic-induced global monsoon drying modulated by diverse El Niño responses, Science Advances, 6, eaba1212, https://doi.org/10.1126/sciadv.aba1212, 2020.

Palmer, W. C.: Keeping Track of Crop Moisture Conditions, Nationwide: The New Crop Moisture Index, Weatherwise, 21, 156–161, https://doi.org/10.1080/00431672.1968.9932814, 1968.

Parker, D. E., Wilson, H., Jones, P. D., Christy, J. R., and Folland, C. K.: The Impact of Mount Pinatubo on World-Wide Temperatures, International Journal of Climatology, 16, 487–497, https://doi.org/10.1002/(SICI)1097-0088(199605)16:5<487::AID-JOC39>3.0.CO;2-J, 1996.

Pinto, J. P., Turco, R. P., and Toon, O. B.: Self-limiting physical and chemical effects in volcanic eruption clouds, Journal of Geophysical Research: Atmospheres, 94, 11165–11174, https://doi.org/10.1029/JD094iD08p11165, 1989.

Polvani, L. M., Banerjee, A., and Schmidt, A.: Northern Hemisphere continental winter warming following the 1991 Mt. Pinatubo eruption: reconciling models and observations, Atmospheric Chemistry and Physics, 19, 6351–6366, https://doi.org/10.5194/acp-19-6351-2019, 2019.

Proctor, J., Hsiang, S., Burney, J., Burke, M., and Schlenker, W.: Estimating global agricultural effects of geoengineering using volcanic eruptions, Nature, 560, 480–483, https://doi.org/10.1038/s41586-018-0417-3, 2018.

Ramachandran, S., Ramaswamy, V., Stenchikov, G. L., and Robock, A.: Radiative impact of the Mount Pinatubo volcanic eruption: Lower stratospheric response, Journal of Geophysical Research: Atmospheres, 105, 24409–24429, https://doi.org/10.1029/2000JD900355, 2000.

Raman, A., Verulkar, S., Mandal, N., Variar, M., Shukla, V., Dwivedi, J., Singh, B., Singh, O., Swain, P., Mall, A., Robin, S., Chandrababu, R., Jain, A., Ram, T., Hittalmani, S., Haefele, S., Piepho, H.-P., and Kumar, A.: Drought yield index to select high yielding rice lines under different drought stress severities, Rice, 5, 31, https://doi.org/10.1186/1939-8433-5-31, 2012.

Ramaswamy, V., Chanin, M.-L., Angell, J., Barnett, J., Gaffen, D., Gelman, M., Keckhut, P., Koshelkov, Y., Labitzke, K., Lin, J.-J. R., O'Neill, A., Nash, J., Randel, W., Rood, R., Shine, K., Shiotani, M., and Swinbank, R.: Stratospheric temperature trends: Observations and model simulations, Reviews of Geophysics, 39, 71–122, https://doi.org/10.1029/1999RG000065, 2001.

https://doi.org/10.5194/egusphere-2024-2280
Preprint. Discussion started: 3 September 2024


Ramaswamy, V., Schwarzkopf, M. D., Randel, W. J., Santer, B. D., Soden, B. J., and Stenchikov, G. L.: Anthropogenic and Natural Influences in the Evolution of Lower Stratospheric Cooling, Science, 311, 1138–1141, https://doi.org/10.1126/science.1122587, 2006.

Robock, A.: Volcanic eruptions and climate, Reviews of Geophysics, 38, 191–219, https://doi.org/10.1029/1998RG000054, 2000.

Robock, A.: Cooling following large volcanic eruptions corrected for the effect of diffuse radiation on tree rings, Geophysical Research Letters, 32, https://doi.org/10.1029/2004GL022116, 2005.

Robock, A. and Liu, Y.: The Volcanic Signal in Goddard Institute for Space Studies Three-Dimensional Model Simulations, Journal of Climate, 7, 44–55, https://doi.org/10.1175/1520-0442(1994)007<0044:TVSIGI>2.0.CO;2, 1994.

Rogers, H. L., Norton, W. A., Lambert, A., and Grainger, R. G.: Transport of Mt. Pinatubo aerosol by tropospheric synoptic-scale and stratospheric planetary-scale waves, Quarterly Journal of the Royal Meteorological Society, 124, 193–209, https://doi.org/10.1002/qj.49712454509, 1998.

Rosenzweig, C. and Abramopoulos, F.: Land-Surface Model Development for the GISS GCM, Journal of Climate, 10, 2040–2054, https://doi.org/10.1175/1520-0442(1997)010<2040:LSMDFT>2.0.CO;2, 1997.

Rosenzweig, C. and Parry, M. L.: Potential impact of climate change on world food supply, Nature, 367, 133–138, https://doi.org/10.1038/367133a0, 1994.

Russell, P. B., Livingston, J. M., Pueschel, R. F., Bauman, J. J., Pollack, J. B., Brooks, S. L., Hamill, P., Thomason, L. W., Stowe, L. L., Deshler, T., Dutton, E. G., and Bergstrom, R. W.: Global to microscale evolution of the Pinatubo volcanic aerosol derived from diverse measurements and analyses, Journal of Geophysical Research: Atmospheres, 101, 18745–18763, https://doi.org/10.1029/96JD01162, 1996.

Santer, B. D., Bonfils, C., Painter, J. F., Zelinka, M. D., Mears, C., Solomon, S., Schmidt, G. A., Fyfe, J. C., Cole, J. N. S., Nazarenko, L., Taylor, K. E., and Wentz, F. J.: Volcanic contribution to decadal changes in tropospheric temperature, Nature Geosci, 7, 185–189, https://doi.org/10.1038/ngeo2098, 2014.

Sato, M., Hansen, J. E., McCormick, M. P., and Pollack, J. B.: Stratospheric aerosol optical depths, 1850–1990, Journal of Geophysical Research: Atmospheres, 98, 22987–22994, https://doi.org/10.1029/93JD02553, 1993.

Scheff, J. and Frierson, D. M. W.: Terrestrial Aridity and Its Response to Greenhouse Warming across CMIP5 Climate Models, https://doi.org/10.1175/JCLI-D-14-00480.1, 2015.

Self, S., Zhao, J.-X., Holasek, R. E., Torres, R. C., and King, A. J.: The Atmospheric Impact of the 1991 Mount Pinatubo Eruption, 1993.

Seneviratne, S. I., Corti, T., Davin, E. L., Hirschi, M., Jaeger, E. B., Lehner, I., Orlowsky, B., and Teuling, A. J.: Investigating soil moisture–climate interactions in a changing climate: A review, Earth-Science Reviews, 99, 125–161, https://doi.org/10.1016/j.earscirev.2010.02.004, 2010.

Sheng, J.-X., Weisenstein, D. K., Luo, B.-P., Rozanov, E., Arfeuille, F., and Peter, T.: A perturbed parameter model ensemble to investigate Mt. Pinatubo's 1991 initial sulfur mass emission, Atmospheric Chemistry and Physics, 15, 11501–11512, https://doi.org/10.5194/acp-15-11501-2015, 2015a.

Sheng, J.-X., Weisenstein, D. K., Luo, B.-P., Rozanov, E., Stenke, A., Anet, J., Bingemer, H., and Peter, T.: Global atmospheric sulfur budget under volcanically quiescent conditions: Aerosol-chemistry-climate model predictions and validation, Journal of Geophysical Research: Atmospheres, 120, 256–276, https://doi.org/10.1002/2014JD021985, 2015b.

Shindell, D. T.: Climate and ozone response to increased stratospheric water vapor, Geophysical Research Letters, 28, 1551–1554, https://doi.org/10.1029/1999GL011197, 2001.

Shindell, D. T., Faluvegi, G., and Bell, N.: Preindustrial-to-present-day radiative forcing by tropospheric ozone from improved simulations with the GISS chemistry-climate GCM, Atmospheric Chemistry and Physics, 3, 1675–1702, https://doi.org/10.5194/acp-3-1675-2003, 2003.

Shindell, D. T., Faluvegi, G., Unger, N., Aguilar, E., Schmidt, G. A., Koch, D. M., Bauer, S. E., and Miller, R. L.: Simulations of preindustrial, present-day, and 2100 conditions in the NASA GISS composition and climate model G-PUCCINI, Atmospheric Chemistry and Physics, 6, 4427–4459, https://doi.org/10.5194/acp-6-4427-2006, 2006.

Sigl, M., Winstrup, M., McConnell, J. R., Welten, K. C., Plunkett, G., Ludlow, F., Büntgen, U., Caffee, M., Chellman, N., Dahl-Jensen, D., Fischer, H., Kipfstuhl, S., Kostick, C., Maselli, O. J., Mekhaldi, F., Mulvaney, R., Muscheler, R., Pasteris, D. R., Pilcher, J. R., Salzer, M., Schüpbach, S., Steffensen, J. P., Vinther, B. M., and Woodruff, T. E.: Timing and climate forcing of volcanic eruptions for the past 2,500 years, Nature, 523, 543–549, https://doi.org/10.1038/nature14565, 2015.

Simard, M., Pinto, N., Fisher, J. B., and Baccini, A.: Mapping forest canopy height globally with spaceborne lidar, Journal of Geophysical Research: Biogeosciences, 116, https://doi.org/10.1029/2011JG001708, 2011.

Singh, R., Tsigaridis, K., LeGrande, A. N., Ludlow, F., and Manning, J. G.: Investigating hydroclimatic impacts of the 168–158 BCE volcanic quartet and their relevance to the Nile River basin and Egyptian history, Climate of the Past, 19, 249–275, https://doi.org/10.5194/cp-19-249-2023, 2023.

https://doi.org/10.5194/egusphere-2024-2280
Preprint. Discussion started: 3 September 2024


Soden, B. J., Wetherald, R. T., Stenchikov, G. L., and Robock, A.: Global Cooling After the Eruption of Mount Pinatubo: A Test of Climate Feedback by Water Vapor, Science, 296, 727–730, https://doi.org/10.1126/science.296.5568.727, 2002.

Stenchikov, G. L., Kirchner, I., Robock, A., Graf, H.-F., Antuña, J. C., Grainger, R. G., Lambert, A., and Thomason, L.: Radiative forcing from the 1991 Mount Pinatubo volcanic eruption, Journal of Geophysical Research: Atmospheres, 103, 13837–13857, https://doi.org/10.1029/98JD00693, 1998.

Tejedor, E., Steiger, N. J., Smerdon, J. E., Serrano-Notivoli, R., and Vuille, M.: Global hydroclimatic response to tropical volcanic eruptions over the last millennium, Proceedings of the National Academy of Sciences, 118, e2019145118, https://doi.org/10.1073/pnas.2019145118, 2021.

Thornthwaite, C. W.: An Approach toward a Rational Classification of Climate, Geographical Review, 38, 55–94, https://doi.org/10.2307/210739, 1948.

Timmreck, C., Graf, H.-F., and Feichter, J.: Simulation of Mt. Pinatubo Volcanic Aerosol with the Hamburg Climate Model ECHAM4, Theor Appl Climatol, 62, 85–108, https://doi.org/10.1007/s007040050076, 1999.

Toohey, M., Krüger, K., Sigl, M., Stordal, F., and Svensen, H.: Climatic and societal impacts of a volcanic double event at the dawn of the Middle Ages, Climatic Change, 136, 401–412, https://doi.org/10.1007/s10584-016-1648-7, 2016.

Toohey, M., Krüger, K., Schmidt, H., Timmreck, C., Sigl, M., Stoffel, M., and Wilson, R.: Disproportionately strong climate forcing from extratropical explosive volcanic eruptions, Nature Geosci, 12, 100–107, https://doi.org/10.1038/s41561-018-0286-2, 2019.

Trenberth, K. E. and Dai, A.: Effects of Mount Pinatubo volcanic eruption on the hydrological cycle as an analog of geoengineering, Geophysical Research Letters, 34, https://doi.org/10.1029/2007GL030524, 2007.

Trenberth, K. E. and Stepaniak, D. P.: The flow of energy through the earth's climate system, Quarterly Journal of the Royal Meteorological Society, 130, 2677–2701, https://doi.org/10.1256/qj.04.83, 2004.

Trenberth, K. E., Fasullo, J. T., and Kiehl, J.: Earth's Global Energy Budget, Bulletin of the American Meteorological Society, 90, 311–324, https://doi.org/10.1175/2008BAMS2634.1, 2009.

Trepte, C. R., Veiga, R. E., and McCormick, M. P.: The poleward dispersal of Mount Pinatubo volcanic aerosol, Journal of Geophysical Research: Atmospheres, 98, 18563–18573, https://doi.org/10.1029/93JD01362, 1993.

Vehkamäki, H., Kulmala, M., Napari, I., Lehtinen, K. E. J., Timmreck, C., Noppel, M., and Laaksonen, A.: An improved parameterization for sulfuric acid–water nucleation rates for

https://doi.org/10.5194/egusphere-2024-2280
Preprint. Discussion started: 3 September 2024


tropospheric and stratospheric conditions, Journal of Geophysical Research: Atmospheres, 107, AAC 3-1-AAC 3-10, https://doi.org/10.1029/2002JD002184, 2002.

Wada, Y., Wisser, D., Eisner, S., Flörke, M., Gerten, D., Haddeland, I., Hanasaki, N., Masaki, Y., Portmann, F. T., Stacke, T., Tessler, Z., and Schewe, J.: Multimodel projections and uncertainties of irrigation water demand under climate change, Geophysical Research Letters, 40, 4626–4632, https://doi.org/10.1002/grl.50686, 2013.

Weng, E., Aleinov, I., Singh, R., Puma, M. J., McDermid, S. S., Kiang, N. Y., Kelley, M., Wilcox, K., Dybzinski, R., Farrior, C. E., Pacala, S. W., and Cook, B. I.: Modeling demographic-driven vegetation dynamics and ecosystem biogeochemical cycling in NASA GISS’s Earth system model (ModelE-BiomeE v.1.0), Geoscientific Model Development Discussions, 1–60, https://doi.org/10.5194/gmd-2022-72, 2022.

van der Werf, G. R., Randerson, J. T., Giglio, L., van Leeuwen, T. T., Chen, Y., Rogers, B. M., Mu, M., van Marle, M. J. E., Morton, D. C., Collatz, G. J., Yokelson, R. J., and Kasibhatla, P. S.: Global fire emissions estimates during 1997–2016, Earth System Science Data, 9, 697–720, https://doi.org/10.5194/essd-9-697-2017, 2017.

Wisser, D., Fekete, B. M., Vörösmarty, C. J., and Schumann, A. H.: Reconstructing 20th century global hydrography: a contribution to the Global Terrestrial Network- Hydrology (GTN-H), Hydrology and Earth System Sciences, 14, 1–24, https://doi.org/10.5194/hess-14-1-2010, 2010.

Zambri, B. and Robock, A.: Winter warming and summer monsoon reduction after volcanic eruptions in Coupled Model Intercomparison Project 5 (CMIP5) simulations, Geophysical Research Letters, 43, 10,920-10,928, https://doi.org/10.1002/2016GL070460, 2016.

Zambri, B., LeGrande, A. N., Robock, A., and Slawinska, J.: Northern Hemisphere winter warming and summer monsoon reduction after volcanic eruptions over the last millennium, Journal of Geophysical Research: Atmospheres, 122, 7971–7989, https://doi.org/10.1002/2017JD026728, 2017.

Zhao, J., Turco, R. P., and Toon, O. B.: A model simulation of Pinatubo volcanic aerosols in the stratosphere, Journal of Geophysical Research: Atmospheres, 100, 7315–7328, https://doi.org/10.1029/94JD03325, 1995.